# Developing a Solid-State Battery Phase-Field Model

by

S. D. Ruis

to obtain the degree of

**Bachelor of Science**
in Applied Physics
and
in Applied Mathematics

to be defended publicly on Monday, November 23, 2020 at 01:30PM.

| | | |
|---|---|---|
| Student number: | 4720717 | |
| Supervisor Applied Physics: | A. Vasileiadis | RST |
| Supervisor Applied Mathematics: | Dr. N. V. Budko | Numerical Analysis |
| Thesis committee: | Prof. Dr. ir. M. Wagemaker, | RST |
| | Dr. L. van Eijck, | RST |
| | Dr. J. G. Spandaw, | Analysis (Colloquium) |

TU Delft

# Abstract

The ongoing worldwide energy transition has prompted significant scientific interest in energy storage. Rechargeable lithium-ion batteries have become a standard for energy storage in mobile devices and electric vehicles for their mass-energy density. While industry standard lithium-ion cells are currently based on liquid electrolytes, solid electrolytes promise to bring the next step towards safety, energy density and sustainability. However, there are critical challenges, notably improving the lithium conduction of solid electrolytes. Furthermore, as a relatively new research field it is important to target high recyclability and sustainability for materials early on. Battery modelling facilitates performance comparisons of for example battery materials and geometric properties, and subsequent optimisation. The report treats battery modelling with a specific focus on solid electrolytes. Two solid electrolyte models, based on weak electrolyte theory and a lattice gas model by Landstorfer et al., were implemented in the Multiphase Porous Electrode Theory software (Smith & Bazant, 2017). The former is relevant for glass type electrolytes, while the latter models crystalline materials. The models showed comparable performance, with a constant voltage offset but good mutual agreement in term of behaviour. It is important to verify the results experimentally. The numerical methods used in porous electrode theory were treated with the creation of a standalone porous electrode model, with separate domains for the electrolyte and active cathode particles. This model is stable and functional with the two domains in isolation, while a fault remains in the coupling between the domains. Lastly, a proposal is made for the addition of interface regions in the MPET software. With these domains situated between the bulk electrolyte and active cathode particles, porous electrode models could include a variety of phenomena that are currently impossible to implement. For solid electrolytes in particular, modelling dynamic stress effects and lithium conduction across particle boundaries would be valuable additions.

# Contents

# 1 Introduction

The global shift towards renewable energy sources is accompanied with increased demand for energy storage. Most renewable energy sources have uncontrollable output, requiring the energy to be stored for later use. Furthermore, as the mobility and transport industry move beyond fossil fuels, a challenging set of properties will be demanded from energy storage solutions. Batteries have a leading role in energy storage, especially when mass-energy density is of importance. Because of the scale of use, marginal gains in mass- and volume-energy density, power density, durability, safety, recyclability and cost will each have a large impact on the effectiveness of batteries in supporting the energy transition. Yet many of the desirable properties are mutually exclusive, making battery design challenging. Currently, lithium-ion batteries with liquid-based electrolytes are the industry standard. To achieve high capacity and energy density, liquid electrolyte submerges an intricate porous electrode with activate particles that host the lithium reaction. However, the liquid is usually flammable and toxic. Solid electrolytes promise to significantly improve the safety and energy density of lithium-ion batteries (Zheng, Kotobuki, Song, Lai, & Lu, 2018). Solid electrolyte usually comes in a powder or glassy form, and the replacement of liquid with solid electrolyte is not straightforward. Lithium diffuses through solid electrolytes in a different way compared to through liquids, and the interaction with electrode materials is also more complicated. Developing a theory for solid electrolytes and using this in a model can be use to gain insight into the ways solid electrolytes and their behaviour differ from liquid electrolytes. The results should be experimentally verified, after which the model can be used to compare different materials, geometrical configurations and conditions in order to improve battery designs.

In this work three paths are taken to improve battery modelling for solid state materials. Firstly, solid state electrolyte physics will be implemented in existing battery simulation software called MPET (Multiphase Porous Electrode Theory (Smith & Bazant, 2017)). This is done using two solid electrolyte models, namely the weak solid electrolyte model and a model formulated by Landstorfer et al.. Next, the numerical methods required for battery modeling are analysed and verified through the development of a standalone porous electrode model. Lastly, interface regions for porous electrode theory are introduced. To this end, the necessary theory is treated in section 2. Section 3 describes the work done on all three topics. In section 4 results are provided and discussed.

# 2 Theory of Battery modelling

Battery modelling is a challenge for a variety of reasons. Even simpler battery models use coupled and often nonlinear partial differential equations to describe the various processes. In this section the important physics to understand battery modeling will be covered.

## 2.1 Fundamentals of electrochemical cells

An electrochemical cell has two electrodes, each of which hosts a half-reaction, resulting in a neutral overall reaction. At the anode an oxidation reaction takes place, and at the cathode a reduction reaction takes place. The electrodes are separated by an electrolyte which is conductive for ions and resistive for electrons. Electrons travel through an external circuit. The oxidised species travels through the electrolyte from the anode to the cathode, where its reduction takes place. A cell in which ions will travel from the anode to the cathode spontaneously, resulting in a positive energy output, is called a galvanic cell. If however an external potential needs to be applied to drive the half-reactions, storing chemical energy in the process, the cell is called electrolytic.
The anode and cathode are named based on the type of half-reaction that occurs. An oxidising electrode is called an anode, and a reducing electrode is called a cathode, hence reversing the reactions would also reverse the nomenclature. There is a widely used convention to always use the electrode names as if the cell is galvanic (discharging). We will use the proper definitions.

The energy provided or consumed by an electrochemical cell is fundamentally expressed by the change in Gibbs free energy per mole the reaction, $\Delta G$. The sign of $\Delta G$ is positive for energy lost to the system and negative for energy gained from the system. The change in free energy can be related to the open circuit potential or *emf* of the cell reaction $E_{cell}$ as follows:

$$\Delta G = -nFE_{cell} \tag{1}$$

where $n$ is the number of moles of electrons per mole of reacted product, and $F = 96.4 \cdot 10^3 \left[\frac{C}{mol}\right]$ is Faraday's constant. Similar to $\Delta G$, $E_{cell}$ is dependent on the direction of the reaction in the cell, with positive open circuit potential indicating a spontaneous reaction and a negative open circuit potential indicating that an external potential has to be applied to drive the reaction. The open circuit potential describes the equilibrium condition where there is no net current flowing. In practice thermodynamic irreversibility leads the actual cell potential to be lower than the emf during discharging (less energy output than the theoretical reversible maximum), and higher than the emf during charging (more energy input than stored in the system). This is called potential hysteresis. The causes for these losses will be described in detail.

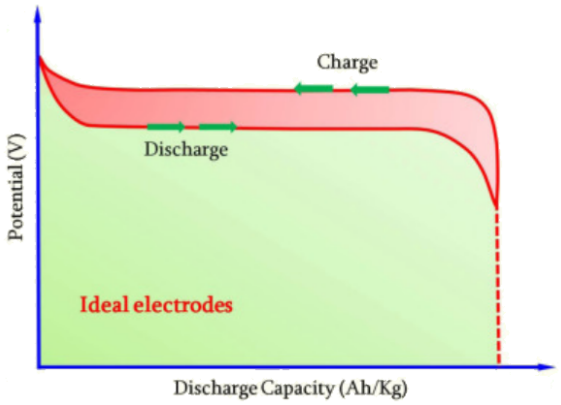


Figure 1: Typical charge and discharge curves showing potential hysteresis. Due to internal energy losses the charging reactions require a higher potential than that which the discharging reactions give in return. Image courtesy of (Liu et al., 2016).

Thin-film batteries have low capacities and are relatively cheap and simple to manufacture, making them suitable for low-capacity applications and research into new battery materials. However, their simple geometry results in a small interface area between the electrolyte and cathode, limiting the discharge current for commercial high capacities. Bulk-type batteries are the solution to this, with their porous anode and cathode consisting of many 'active particles' submerged in electrolyte. The active particles host the half reactions, greatly improving the reactive surface area. Additives such as particle coatings are often used at the anode and cathode to enhance the transfer of charged particles to and from the electrolyte. There are differences in the modelling of thin-film and bulk-type batteries, which will be discussed later. A schematic comparison of the architectures is given in figure 2.

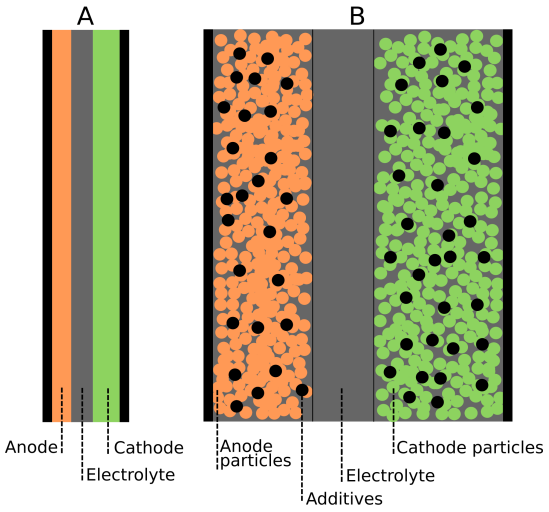


Figure 2: A: Schematic of a thin-film battery. The interfaces between the components are straight. B: Schematic of a bulk-type battery with porous electrodes.

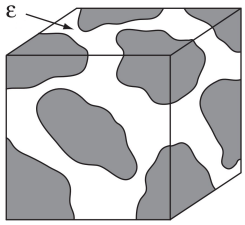


Figure 3: Schematic of a porous electrode volume. (Bazant, 2012)

## 2.2 Porous electrodes

The three essential parts of a porous electrode are active material, conducting material and binding agents that together form a solid matrix. Conductive material is required to transport electrons from deep in the electrode to the current collectors. Active material hosts the half-reactions of the battery. Graphite is a common active material in anodes, in cathodes iron phosphate ($FePO_4$) is often used. Carbon black is used as conducting material (Bazant, 2012). When liquid electrolyte is added, it reaches all the pores in the matrix yielding a large reactive area. When using this system there are a number of properties of importance for modelling and optimizing the performance and efficiency of the electrodes. Firstly, the porosity of an electrode is denoted by $\epsilon$, and defined by the volume fraction of electrolyte in the electrode. $\epsilon = 1$ indicates pure electrolyte. The region of pure electrolyte in a porous electrode battery is often called a separator. The solid matrix takes a portion of the volume, lowering the porosity below 1. Lower porosity in an electrode will give a higher capacity as more active material can be present, but performance could be hampered by a lack of electrolyte transporting the lithium to the active particles. Electrode length is also a parameter that gives a compromise between capacity and performance, as diffusing lithium a long distance through the porous medium comes at the cost of efficiency.

## 2.3 Overpotential

An overpotential is a difference between a half reaction's potential given by ideal thermodynamics and the observed potential. There exist a variety causes for overpotentials, all connected to a specific non-ideal aspect or limiting process in the battery. The main examples are activation overpotential, concentration overpotential and the ohmic drop. Activation overpotential is the difference from the equilibrium potential required to produce a current at an electrode. It refers to the activation energy barrier that electrons must traverse to take part in the redox reaction. A greater current will require a greater overpotential, changing the net potential of the half reaction. In this work the Butler-Volmer equation will be used to relate the activation overpotential to a current density:

$$\boldsymbol{j} = \boldsymbol{i}_0 \left[ exp\left( \frac{(1-\alpha)e\eta}{k_B T} \right) - exp\left( -\frac{\alpha e \eta}{k_B T} \right) \right] \tag{2}$$

Here $\boldsymbol{j}$ is the current density in $\frac{A}{m^2}$, positive $\boldsymbol{j}$ indicates a net oxidation reaction, with ions being released into the electrolyte. The left term in the square brackets is the anodic current, representing the oxidation reaction. The right term is the cathodic current representing the reduction reaction. When the overpotential becomes negative, the anodic reaction decreases and the cathodic reaction increases, resulting in a negative $\boldsymbol{j}$. $\boldsymbol{i}_0$ is the exchange current density, the equal current that is flowing in both directions when the overpotential is zero. $e$, $k_B$, and $T$ are the familiar electron charge, Boltzmann constant and standard temperature of $298°K$ respectively. $\alpha$ is the dimensionless charge transfer coefficient, determining the relative requirement for overpotential for the anodic and cathodic currents. Figure 4 shows the Butler-Volmer equation for $\alpha = 0.5$ and its decomposition in anodic and cathodic currents.

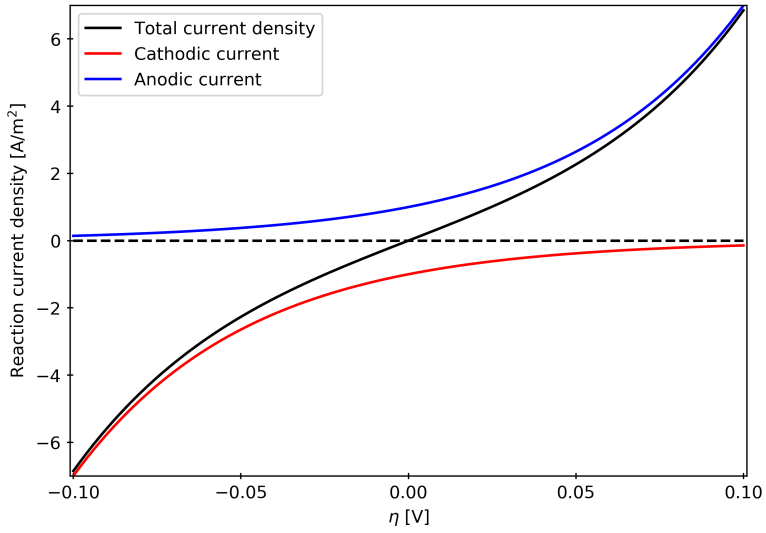


Figure 4: The relationship between activation overpotential and reaction current according to Butler-Volmer kinetics. At $\eta = 0$ there is equal current in both directions (anodic and cathodic).

Comparatively, the activation overpotential will be dominant at low currents because the concentration overpotential is negligible in that case. The concentration overpotential refers to energy losses due to limits in the transport of ions through the electrolyte. At high currents the

concentration overpotential becomes significant. Lastly, the ohmic drop refers to the resistance an electron encounters when traversing the solid matrix of the cathode to an active particle. This resistance leads to efficiency loss and heat generation, especially in long cathodes in which electrons have to travel further through the solid matrix. In many cases the ohmic drop is negligible, and while the MPET model does take it into account it was left out of the standalone model for simplicity.

## 2.4 C-rate

With the knowledge of overpotentials it becomes understandable that a battery's voltage output is dependent on the current demand. This means there is a choice of independent variable when running a battery model. With a discharging model, either one demands a fixed current from the battery and the resulting voltage is of interest, or the voltage is fixed and the resulting current is the model output. These models are called Constant Current (CC) or Constant Voltage (CV) respectively. Constant Current is the most common method, and will be used in this report. The magnitude of the constant current is denoted by the C-rate, defined as the current divided by the theoretical current required to fully (dis)charge the battery in one hour. For example, a 6C discharge current would fully discharge the battery in 10 minutes, and C/2 means the battery would be discharged in 2 hours. Describing the current demand using C-rate allows for straightforward comparison of different sizes and types of batteries, without having to know the specific currents.

## 2.5 Phase fields and statistical thermodynamics for batteries

Both the electrolyte and the active particles have complex microstructures, and it is impossible to model these down to the atomic level. What is needed is a method to compute aspects of the microstructure without explicitly modelling the complete system. The Phase field method makes this possible, by encapsulating the condition of the microstructure in a single variable known as an order parameter, denoted by $\phi$. Order parameters take a value between 0 and 1, and vary continuously throughout the domain. A simple example of the phase field method working to simplify a problem would be the formation of precipitate in a solution through an interface. With the phase field method, the precipitate, solution and interface are given by $\phi = 1$, $\phi = 0$ and a region where $0 < \phi < 1$ respectively. These values together are the phase field. $\phi$ and its gradients, are used to define a thermodynamic function of state, such as the free energy. The change of the system in time rests on how the thermodynamic function of state changes with $\phi$. In the figures below the resulting phase field description is visualised for a smooth and sharp interface. Another advantage of phase fields is that the location and shape of the interface are emergent from the model, and thus there is no need to describe them through explicit mathematical equations (Moelans, Blanpain, & Wollants, 2008).

The appropriate thermodynamic function of state will depend on the definition of the problem. The Gibbs free energy $G$ is appropriate for isothermal systems at constant pressure, and will be used here. Entropy and Helmholz free energy are used for other problems. $G$ is only explicitly defined for systems of homogeneous phase, while heterogeneous systems are of interest. Cahn and Hilliard proved that when $G(\phi, \nabla\phi, \nabla^2\phi, \ldots)$ is a function of the order parameter and its derivatives, a multivariate Taylor expansion around the homogeneous Gibbs free energy $G_0$ can be used to calculate the heterogeneous $G$ (Cahn & Hilliard, 1958).

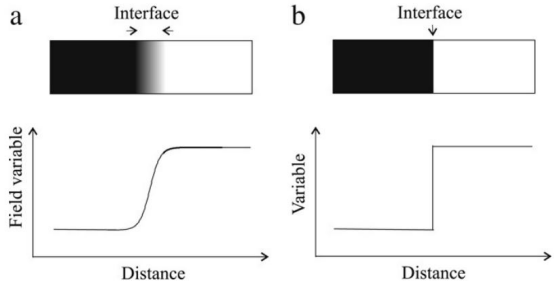


Figure 5: The evolution in space of an interface expressed using the phase field method. a) is a smooth interface, b) is sharp.(Qin & Bhadeshia, 2010)

The result of the derivation in (Qin & Bhadeshia, 2010) is the following integral:

$$G[\phi] = \int_V \left[ g_o(\phi, T) + \frac{\varepsilon^2}{2}(\nabla\phi)^2 \right] dV \tag{3}$$

Where $g_0$ is the Gibbs free energy of the homogeneous system per unit volume. The gradient energy coefficient $\varepsilon^2$ is equal to:

$$\varepsilon^2 = \frac{\partial^2 g_0}{\partial(\nabla\phi)^2} - 2\frac{\partial^2 g_0}{\partial\phi\partial\nabla^2\phi} \tag{4}$$

This result means that the free energy of a volume is composed of two primary contributions, namely the free energy of the volume in a homogeneous phase, and a gradient term. The gradient energy coefficient contains the interface properties for the system, such as its energy per unit area.

In the case of electrolyte or active particles, the order parameter of choice is the dimensionless concentration of the solute species, in this case lithium, denoted by $\tilde{c} = \frac{c}{c_{max}}$. $\tilde{c}$ indeed varies between 0 and 1, and it can be used to write down the free energy functional.

Since $\tilde{c}$ represents a concentration, and the change in time of the concentration must follow the mass conservation equation:

$$\frac{\partial \tilde{c}}{\partial t} = -\nabla \cdot \boldsymbol{F} \tag{5}$$

Onsager derived that the driving force for the mass flux is the gradient of the chemical potential (Monroe & Newman, 2007):

$$\boldsymbol{F} = -\boldsymbol{M} \nabla \mu \tag{6}$$

Where $\boldsymbol{M}$ is the mobility tensor, which can be assumed to reduce to a scalar mobility $M$ for the current purpose. The chemical potential is defined as the variational derivative of $G$ with respect to $\tilde{c}$ (Provatas & Elder, 2010, p. 36):

$$\mu = \frac{\delta G}{\delta \tilde{c}} = \bar{\mu}(\tilde{c}) - \nabla \cdot (\varepsilon \nabla \tilde{c}) \tag{7}$$

By combining equations 5, 6 and 7 the Cahn-Hilliard equation is found.

$$\frac{\partial \tilde{c}}{\partial t} = \nabla \cdot \left( M \nabla \frac{\delta G}{\delta \tilde{c}} \right) \tag{8}$$

The mobility is proportional to the diffusivity according to the Einstein relation:

$$M = \frac{D}{k_B T} \tag{9}$$

Fundamentally the Cahn-Hilliard equation relates the free energy of lithium in the system to the evolution of the concentration over time. It will become clear that in the electrolyte there is in fact no phase separation, and while using phase field methods to derive the partial differential equations that hold in the electrolyte is not wrong, it is not strictly necessary. The phase field method will show its potential when modeling the active particles, which do show phase separation, as well as when modeling interface regions between particles and bulk electrolyte.

## 2.6 Electrolyte transport equations

We derive the equations used to describe the mass transport and current in the electrolyte according to porous electrode theory. The variables of interest, called field variables, are the concentration $c$, electric potential $\phi$, current density $\boldsymbol{i}$ and lithium consumption $j_{in}$.
All the forthcoming holds for a species $i$ in the electrolyte. For the current case, the species of interest are lithium and electrons. The electrochemical potential of $i$ consists of a contribution from the chemical activity $a_i$ and an electrostatic contribution:

$$\mu_i = k_B T \ln(a_i) + z_i e \phi \tag{10}$$

The chemical activity is a dimensionless effective concentration defined as the product of the activity coefficient $\gamma_i$ and the concentration $c_i$. The term $k_B T \ln(\gamma_i)$ represents the deviation in electrochemical potential from a defined standard condition, which is a customary choice. $z_i$ is the number of elementary charges $e$ carried by species $i$, which can be negative. $\phi$ is the electrical potential. Plugging 10 into a dimensional version of the mass flux equation 6, the derivative of $\ln(a_i)$ is worked out as shown below,

$$\begin{aligned} D_i c_i \frac{\partial \ln(a_i)}{\partial x} = D_i \left( \frac{\partial c_i}{\partial x} + \frac{c_i}{\gamma_i} \frac{\partial \gamma_i}{\partial x} \right) = D_i \left( 1 + \frac{c_i}{\gamma_i} \frac{\partial \gamma_i}{\partial c_i} \right) \frac{\partial c_i}{\partial x} = \\ = D_i \left( 1 + \frac{\partial \ln \gamma_i}{\partial \ln c_i} \right) \frac{\partial c_i}{\partial x} = D_{chem,i} \frac{\partial c_i}{\partial x} \end{aligned} \tag{11}$$

leading to the chemical diffusivity of species $i$, $D_{chem,i}$. It shows the concentration dependence of the diffusivity due to particle interactions at high concentrations. The vanishing difference between $a_i$ and $c_i$ in the dilute limit also recovers the constant diffusivity as $\gamma_i$ will go to 1. The mass flux equation is as follows:

$$\boldsymbol{F}_i = -D_{chem,i} \nabla c_i - \frac{e z_i}{k_B T} D_i c_i \nabla \phi \tag{12}$$

Equations of this type are Nernst-Planck equations. The first term on the right represents transport of species $i$ due to diffusion, the right term represents electric migration. It is a convection-type term. When two species with equal and opposite charge comprise the electrolyte, the electrolyte is called binary. Since this is the case in a lithium-ion battery, we arrive at two mass flux equations denoted with subscript $+$ for lithium and $-$ for electrons. From equation 13 onward $z_+$ and $z_-$ are the absolute value of the charge numbers, as different signs are used in front of the migration term.

$$\begin{aligned} \boldsymbol{F}_+ &= -\epsilon D_{chem,+} \nabla c_+ - \frac{e z_+}{k_B T} \epsilon D_+ c_+ \nabla \phi \\ \boldsymbol{F}_- &= -\epsilon D_{chem,-} \nabla c_- + \frac{e z_-}{k_B T} \epsilon D_- c_- \nabla \phi \end{aligned} \tag{13}$$

The $\epsilon$ term is the porosity of the electrolyte, the mass flux is multiplied by it because the species can only move through that fraction of the volume which is electrolyte. The mass conservation equations will be of the form

$$\epsilon \frac{\partial c_\pm}{\partial t} = -\nabla \cdot \boldsymbol{F}_\pm - R_\pm \tag{14}$$

Notice the reaction term $R_\pm$ is not multiplied by the porosity. With the given expressions for mass flux, the two mass conservation equations contain the three field variables $c_+$, $c_-$ and $\phi$,

so another equation is necessary to solve the system. This equation is Poisson's equation for electrostatics, derived from Gauss's law.

$$\nabla \cdot \boldsymbol{E} = \frac{\rho}{\epsilon_p} \tag{15}$$

Substituting the definition of the electric field $\boldsymbol{E} = -\nabla\phi$, we obtain Poisson's equation for electrostatics:

$$\nabla^2\phi = -\frac{\rho}{\epsilon_p} = -\frac{e(c_+ - c_-)}{\epsilon_p} \tag{16}$$

Here $\rho$ is the charge density and $\epsilon_p$ the permittivity of the medium, with the subscript to avoid confusion with the porosity $\epsilon$. With the two Nernst-Planck equations, the Poisson equation and appropriate boundary conditions the system can be solved. The equations are collectively called Poisson-Nernst-Planck (PNP) equations. They capture the phenomenon of diffuse charge, caused by the concentrations of lithium atoms and electrons being different at the same location. This happens near the boundary between the electrolyte and active particle, where an electrical double layer is formed, and thus these boundaries have to be specified. PNP equations are used regularly for geometrically simple systems, such as thin-film batteries. In thin-film batteries the interfaces between the electrolyte and the other elements such as the cathode are straightforward to describe mathematically, a single point in one dimension or a single function in two dimensions. Porous electrodes on the other hand have a complex three dimensional mesostructure, and the boundaries between the electrolyte and active particles is exceedingly difficult if not impossible to describe mathematically. Porous electrode theory masks the geometry of the interface by using a source term for the reaction rate. But without the boundary conditions diffuse charge cannot be modeled, and the PNP equations are overly general. The required approximation is electroneutrality. The assumption of electroneutrality implies that

$$\sum_i z_i c_i = 0 \tag{17}$$

everywhere. Hence in the binary electrolyte we have $c_+ = c_-$. This is not a law of nature, instead it results from the prefactor $\frac{e}{\epsilon_p}$ in Poisson's equation, which when multiplied by the Avogadro number becomes of order $10^{16}$ for one molar unit deviation from electroneutrality. The electric field caused by this amount of diffuse charge would cause similarly large forces on the particles, causing redistribution that equalises the charge again. In other words, a negligibly small deviation from electroneutrality would cause a comparatively large electric field working to counter the imbalance of charge, hence preventing significant deviations from electroneutrality (Newman, 2004). However, electroneutrality is not equivalent to replacing Poisson's equation by Laplace's equation $\nabla^2\phi = 0$. The proper approach is to replace Poisson's equation altogether, instead moving forward with a single concentration given by $c = c_+ = c_-$.
With the assumption of electroneutrality in the electrolyte the mass balance equation can be expressed in equal contributions of $c_+$ and $c_-$:

$$\begin{aligned}\epsilon\frac{\partial c}{\partial t} = \epsilon\frac{1}{2}\frac{\partial}{\partial t}(c_+ + c_-) = \frac{1}{2}\nabla\cdot(\epsilon(D_+ + D_-)\nabla c) \\ + \frac{1}{2}\frac{e\epsilon}{k_B T}(z_+ D_+ - z_- D_-)\nabla\cdot(c\nabla\phi) - \left(\frac{z_+ R_+}{2} + \frac{z_- R_-}{2}\right)\end{aligned} \tag{18}$$

Defining the total current density i as the difference between the two flux densities multiplied by their species' charge, equation 19 is obtained.

$$\mathrm{i} = ez_+\boldsymbol{F}_+ - ez_-\boldsymbol{F}_- = -e\epsilon(D_+ - D_-)\nabla c - \frac{e^2\epsilon}{k_B T}(z_+ D_+ + z_- D_-)c\nabla\phi \tag{19}$$

The structure of equation 19 is reflected in equation 18, and by factoring $\frac{1}{2}\left(\frac{z_+D_+ - z_-D_-}{z_+D_+ + z_-D_-}\right)\frac{\mathrm{i}}{e}$ out of 18 the potential can be eliminated, arriving at the mass conservation equation 20.

$$\epsilon\frac{\partial c}{\partial t} = \nabla\cdot(\epsilon D_{amb}) - \nabla\cdot\left(\left(\frac{t_+ - t_-}{2}\right)\frac{\mathrm{i}}{e}\right) - \left(\frac{z_+R_+}{2} + \frac{z_-R_-}{2}\right) \tag{20}$$

Here $t_+$ and $t_-$ are the lithium and electron transference numbers, defined as the fraction of total electrical current carried by a given species.

$$t_\pm = \frac{z_\pm D_\pm}{z_+D_+ + z_-D_-} \tag{21}$$

In binary electrolytes, $t_+ + t_- = 1$. In solid electrolytes the lithium transference number is often close to 1, because the electrons are nearly immobile. In liquid electrolytes both lithium and electrons cause a significant fraction of the charge transport. $D_{amb}$ is the ambipolar diffusivity, obtained by starting from the $(D_+ + D_-)$: in front of $\nabla c$ in equation 18 and subtracting the $(D_+ - D_-)(t_+ - t_-)$ that was added by introducing $i$ in equation 20, and simplifying.

$$D_{amb} = \frac{(z_+ + z_-)D_+D_-}{z_+D_+ - z_-D_-} \tag{22}$$

More intuitively, the ambipolar diffusivity is the harmonic mean of $D_+$ and $D_-$ weighted by the opposite charge number.

$$\frac{1}{D_{amb}} = \frac{z_-}{z_+ + z_-}\frac{1}{D_+} + \frac{z_+}{z_+ + z_-}\frac{1}{D_-} \tag{23}$$

It is dominated by the species with lower diffusivity or smaller charge number, because the species with higher charge or diffusivity will respond faster to the coulomb force, letting the effective diffusivity be determined by the species that transports charge slowest.

Charge in the electrolyte is conserved, and thus the reaction rates $R_\pm$ can be related to the divergence of the current i. $R$ is the rate of species consumption from the electrolyte, so we have:

$$ez_+R_+ - ez_-R_- = -\nabla\cdot\mathrm{i} = a_p e j_{in} \tag{24}$$

Here $j_{in}$ is the flux density of charged species entering a particle through its outer surface. Multiplied by $e$ gives the current density. $a_p$ represents the particle surface area per unit volume of particles. Substituting $a_p j_{in}$ for the reaction rates $R_\pm$ in equation 20 and rearranging gives the final mass balance:

$$\epsilon\frac{\partial c}{\partial t} = \nabla\cdot(\epsilon D_{amb}\nabla c) - \nabla\cdot\left(\frac{t_+\boldsymbol{i}}{e}\right) - a_p j_{in} \tag{25}$$

By applying equation 24 to equation 19 by taking its divergence we also obtain an equation that can be used to solve for the local electrolyte potential.

$$a_p j_{in} = (D_+ - D_-)\epsilon\nabla^2 c + \frac{e}{k_B T}(z_+D_+ + z_-D_-)\epsilon\nabla\cdot(c\nabla\phi) \tag{26}$$

Equations 24, 25, 26 and the Butler-Volmer equation 2 form the set of equations for porous electrode theory. In section 3 the boundary conditions, and specific modifications for the present application will be discussed.

## 2.7 Active material

The main active material in the model is $FePO_4$, which takes up lithium ions according to the following reaction:

$$x\mathrm{Li}^+ + xe^- + \mathrm{FePO_4} \underset{discharge}{\overset{charge}{\rightleftharpoons}} \mathrm{Li}_x\mathrm{FePO_4} \tag{27}$$

Here $x$ is called the filling fraction and has a value between 0 and 1. The process of filling a particle with lithium is called lithiation.

For the diffusion of lithium through the active particle, we start again with the mass flux expression from concentrated solution theory:

$$\boldsymbol{F}_i = -M_i c_i \nabla \mu_i \tag{28}$$

To obtain an expression for the electrochemical potential the general solution model is used. This starts from an expression of the free energy of a system of ions and vacancies on a lattice (Balluffi, Allen, & Carter, 2005):

$$g = k_B T[\tilde{c}_s \ln \tilde{c}_s + (1 - \tilde{c}_s)\ln(1 - \tilde{c}_s)] + \Omega \tilde{c}_s(1 - \tilde{c}_s) \tag{29}$$

Here $\tilde{c}_s = \frac{c_s}{c_{s,max}}$ is the nondimensional concentration, or composition parameter of the solution. The rightmost term is the entropy of mixing, with $\Omega$ the regular solution parameter. With a higher entropy of mixing the system will tend to produce two phases of differing concentrations. The critical value for $\Omega$ is $2k_BT$, $\Omega > 2k_BT$ implies phase separation while $\Omega < 2k_BT$ implies a homogeneous solution. Figure 6 shows the appearance of two minima in the free energy when $\Omega$ passes the critical value, leading to phase separation. In figure 7 the time evolution of an intercalating particle is shown. It is referred to as the shrinking core model, because the region of low lithium concentration is a sphere concentric with the particle, and shrinks as the particle intercalates.

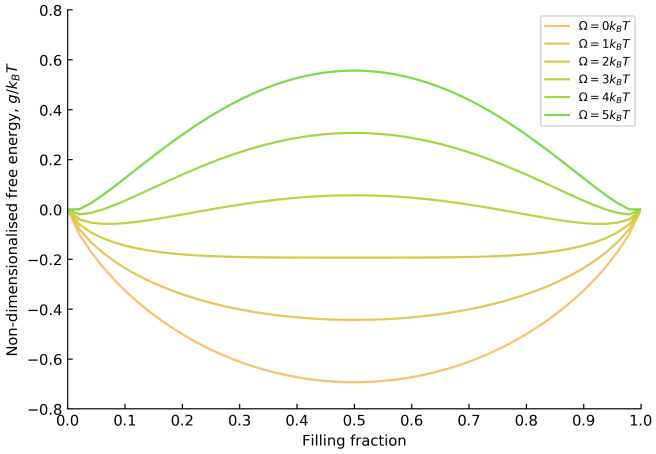


Figure 6: The effect of the regular solution parameter $\Omega$ on the free energy versus composition of a solution of atoms and vacancies on a lattice. For $\Omega < 2k_BT$ there is a single minimum, corresponding to a homogeneous particle. When $\Omega > 2k_BT$ there are two minima, leading to phase separation in the particle, with one region having the smaller composition parameter and the other the larger composition parameter.

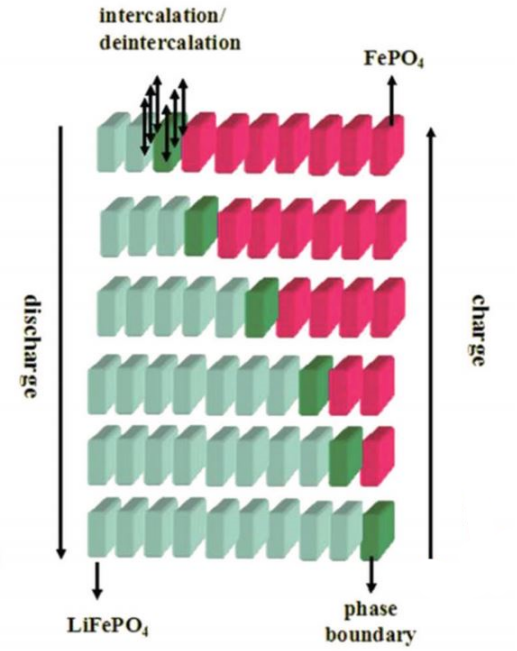


Figure 7: Visualisation of the travelling phase boundary in an iron phosphate particle. Image reproduced from (Wu et al., 2016).

The slope of the free energy is the chemical potential. In a homogeneous regime the slope is strictly increasing, leading to a strictly decreasing voltage profile. In the phase separating regime the slope of $g$ is non-monotonic. This contributes to the voltage plateau of $FePO_4$ and other phase separating materials. After the derivation given in appendix A results in the following nonlinear diffusion equation:

$$\frac{\partial c_s}{\partial t} = \nabla \cdot (D_{chem,s} \nabla c_s) \tag{30}$$

with

$$D_{chem,s} = D_0(1 - 2\tilde{\Omega}\tilde{c}_s + 2\tilde{\Omega}\tilde{c}_s^2) \tag{31}$$

where $\tilde{\Omega} = \Omega / k_B T$.

## 2.8 Solid electrolytes

A variety of materials have emerged as candidates for a solid electrolyte. Most materials can be assigned to two categories, namely organic solid electrolytes that are often polymer based, and inorganic solid electrolytes which can be subdivided into crystalline and glassy materials. Crystal microstructures are periodic, while the microstructure of glass is amorphous, meaning random or without a repeated unit cell. A final variant of solid electrolyte is glass-ceramic, made by crystallisation of a glass precursor. These categories each have their advantages and disadvantages (Bachman et al., 2015). The ionic conductivity is still limiting for the majority of current materials. This limits them to use in thin-film batteries. Glassy and glass ceramic materials generally have a slightly lower ionic conductivity then crystalline electrolytes (Minami, 2005). On the other hand, production of glassy materials could be cheaper and easier because no exotic elements such as germanium are needed. The model proposed here is suited to glassy electrolytes. Another model was implemented in MPET that is more suited to crystalline electrolytes, its derivation is given in appendix B. The lithium conduction in glassy and glass ceramic materials can be modeled using a weak electrolyte model (Ingram, Moynihan, & Lesikar, 1980), which will be described here.

### 2.8.1 Glassy electrolytes: the weak electrolyte model

The amorphous structure of glassy electrolytes determines the number of host sites where lithium is bound to the structure. The concentration of host sites is denoted by $c_0$ At absolute zero temperature, lithium is bound to all host sites in the material. When the temperature is increased, ionisation starts to occur and lithium ions become separated from the structure (Raijmakers, Danilov, Eichel, & Notten, 2020) . Lithium in this interstitial phase, denoted as $Li^+$ is free to diffuse through the electrolyte. An uncompensated negative charge is left at the vacancy. This negative charge is practically immobile, as the electrolyte is a very poor conductor of electrons. The reversible reaction is described by:

$$\mathrm{Li_o} \underset{k_r}{\overset{k_d}{\rightleftharpoons}} \mathrm{Li^+} + e^- \tag{32}$$

where $\mathrm{Li_o}$ denotes the immobile lithium in the microstructure, $\mathrm{Li^+}$ denotes the interstitial (mobile) lithium and $n^-$ denotes the resulting negatively charged vacancies. $k_d$ and $k_r$ are the rate constants for the ionisation and recombination reactions respectively. $c_{\mathrm{Li^+}}$, $c_{\mathrm{Li_o}}$ and $c_{\mathrm{n\text{-}}}$ denote the concentration of mobile Li ions, immobile lithium and negative vacancies respectively. Let $\delta$ be the fraction of lithium that is ionised at equilibrium, the equilibrium mobility fraction. Then at equilibrium it holds that $c_{\mathrm{Li^+}} = c_{\mathrm{n\text{-}}} = \delta c_0$, and the immobile lithium concentration follows as $c_{\mathrm{Li_o}} = (1-\delta)c_0$. The microstructure reaction rate $r$, is given by :

$$r = k_d c_{\mathrm{Li_o}} - k_r c_{\mathrm{Li^+}} c_{\mathrm{n\text{-}}} \tag{33}$$

At equilibrium $r = 0$, and hence $k_d$ can be expressed in terms of $k_r$ using equation 33 and the equilibrium conditions, giving:

$$k_d = \frac{k_r c_0 \delta^2}{(1-\delta)} \tag{34}$$

A host site is either vacant or occupied, so we must have that

$$c_{\mathrm{Li_o}} + c_{\mathrm{Li^+}} = c_0 \tag{35}$$

And by the electroneutrality approximation it holds that

$$c_{\mathrm{Li^+}} = c_{\mathrm{n\text{-}}} \tag{36}$$

Combining these two conditions and the expression 34 for $k_d$ we arrive at the final version of the microstructure reaction rate:

$$r = \frac{k_r c_0 \delta^2}{(1-\delta)}(c_0 - c_{\text{Li}^+}) + k_r c_{\text{Li}^+}^2 \tag{37}$$

To incorporate a glassy solid electrolyte in the MPET model and study influence on the performance, the microstructure reaction rate term is added to the mass balance equation 25.

# 3 Modelling

The performance and behaviour of solid electrolytes in bulk type lithium-ion batteries was studied and compared to conventional liquid electrolytes. The existing MPET model was adapted to include the two solid electrolyte models, discussed in the previous section and appendix B, for both mutual comparison and comparison to the existing liquid electrolyte model. Secondly, the system of equations for Porous Electrode Theory was further explored through the creation of a standalone battery model, adding another source to compare results with. Furthermore, interface regions are introduced as a method to extend the MPET model to better include physics in the interface region between active particles and the solid electrolyte.

## 3.1 Solid electrolyte MPET model

The glassy electrolyte model implemented by adding the microstructure reaction term to mass balance equation 25 in the MPET software. The host site concentration $c_0$ was set to $35.890 \cdot 10^3$ $[\frac{\text{mol}}{\text{m}^3}]$ with an equilibrium mobility fraction of $\delta = 0.4$, and the recombination rate $k_r$ was taken as $8.00 \cdot 10^-7$ $[\frac{\text{m}^3}{\text{mol s}}]$ (Raijmakers et al., 2020). The diffusivities are taken at $D_+ = 1.18 \cdot 10^{-11}$ and $D_- = 1.38 \cdot 10^-12$ $[\frac{\text{m}^2}{\text{s}}]$ (Bachman et al., 2015). For most solid electrolytes the diffusivities are still lower, so these assume state of the art solid electrolyte. The electron diffusivity is nearly one order of magnitude smaller so the lithium transference number will be around 0.9.
The model was run at three discharge rates, $5C$, $1C$ and $C/5$ representing fast, normal and slow discharge respectively. These runs we done once for a cathode length of $100\mu$m, which is industry standard, and a shorter length of $30\mu$m. The separator length was set to $25\mu$m, with 10 volumes for both the separator and cathode, and 3 particles simulated per cathode volume. The spherical particles had a length of 100nm with a standard deviation of 1nm.
Furthermore, at a cathode length of $100\mu$m the dependency of the performance on the equilibrium mobility fraction $\delta$ and the recombination rate $k_r$ were studied by running the model at the same three discharge rates with a spread of $\delta$ and $k_r$.

## 3.2 Standalone porous electrode model

To deepen the understanding of the workings of the MPET model, a standalone battery model was coded in Python using only Scipy's linear solution algorithms. The system of partial differential equations stated in section 2 was discretised using finite difference methods and solved with a segregated solution algorithm. To solve for the reaction rates of different particles a non-linear solver was built using Newton's method. A detailed description of the approach and assumptions will be given this section, and the model's results and behaviour will be compared to the existing model. Once a stable baseline model with liquid electrolyte physics is working, modifications such as solid electrolyte physics and changes to the particle size and distribution can be implemented.

### 3.2.1 Set of equations

The set of equations is similar to that of the MPET model. Let the number of simulated active particles be $P$. There are $P$ one-dimensional domains of length $R$, the length of the modeled particles. In addition there is a single one-dimensional domain with length $L$ equal to the total battery length in which the electrolyte field variables are simulated. There are the four field variables, each with their own equation. There is a coupling to the fifth equation that describes the diffusion in the active particles. The complete set is displayed in table 1 for reference.

Table 1: Set of equations used in the porous electrode model, including their boundary conditions. Each equation is used to solve for its dependent variable.

| # | Dependent variable [unit] | Equation | Boundary conditions |
|---|---|---|---|
| (T1.1) | Concentration $c$ $\left[\frac{1}{\mathrm{m}^3}\right]$ | $\frac{\partial c}{\partial t} = D_{amb}\frac{\partial^2 c}{\partial x^2} - \frac{\partial}{\partial x}\left(\frac{t_+ \boldsymbol{i}}{e\epsilon}\right) - \frac{a_p j_{in}}{\epsilon}$ | $\frac{\partial c}{\partial x}\vert_{x=0} = \frac{I}{AD_+}$<br>$\frac{\partial c}{\partial x}\vert_{x=L} = 0$ |
| (T1.2) | Electric potential $\phi$ $[V]$ | $a_p j_{in} = (D_+ - D_-)\epsilon\frac{\partial^2 c}{\partial x^2} + \frac{e}{k_B T}(z_+ D_+ + z_- D_-)\epsilon\frac{\partial}{\partial x}\left(c\frac{\partial \phi}{\partial x}\right)$ | $\phi\vert_{x=0} = \phi_A$<br>$\frac{\partial \phi}{\partial x}\vert_{x=L} = 0$ |
| (T1.3) | Current density $\boldsymbol{i}$ $\left[\frac{\mathrm{A}}{\mathrm{m}^2}\right]$ | $\boldsymbol{i} = -e(D_+ - D_-)\epsilon\frac{\partial c}{\partial x} - \frac{e^2}{k_B T}(z_+ D_+ + z_- D_-)\epsilon c\frac{\partial \phi}{\partial x}$ | $\boldsymbol{i}\vert_{x=0} = \frac{I}{A}$ $\boldsymbol{i}\vert_{x=0} = 0$ |
| (T1.4.1) | Reaction rate $j_{in,i}$ $\left[\frac{1}{\mathrm{m}^2\mathrm{s}}\right]$ | $e\ j_{in,i} = \boldsymbol{i}_0\left[exp\left(-\frac{\alpha e\eta_i}{k_B T}\right) - exp\left(\frac{(1-\alpha)e\eta_i}{k_B T}\right)\right]$ | $\sum_i V_i a_p j_{in,i} = I$ |
| (T1.4.2) | $[V]$ | $\eta_i = \Delta\phi_i - \Delta\phi_{eq,i}$ | $\phi_i + \Delta\phi_i + \eta_i =$<br>$\phi_j + \Delta\phi_j + \eta_j \quad \forall i, j$ |
| (T1.4.3) | $[V]$ | $\Delta\phi_{eq,i} = V^0 - \frac{k_B T}{e}\ln\left(\frac{\tilde{c}_{s,i}}{1-\tilde{c}_{s,i}}\right) - \frac{\Omega}{e}(1 - \tilde{c}_{s,i})$ | - |
| (T1.5) | Active particle concentration $c_{s,i}$ $\left[\frac{1}{\mathrm{m}^3}\right]$ | $\frac{\partial c_s}{\partial t} = \frac{\partial}{\partial r}\left(D_{chem,s}\frac{\partial c_s}{\partial r}\right)$ | $\frac{\partial c_{s,i}}{\partial r}\vert_{r=0} = j_{in,i}$<br>$\frac{\partial c_{s,i}}{\partial r}\vert_{r=R} = 0$ |

Equation T1.1 is the mass conservation equation with Neumann boundary conditions. On the left the inward flux is the specified constant current (CC) value $I$ divided by the battery area $A$ and the lithium diffusion coefficient $D_+$, since only lithium is entering the electrolyte at the anode. The right BC is zero, since there is no exchange of matter between the electrolyte and the cathode current collector.
The electrode potential equation T1.2 is derived from the expression for the current T1.3 and realising that charge conservation relates the current's divergence to the reaction rate $j_{in}$ according to equation 38:

$$j_{in} = -\frac{1}{ea_p}\frac{\partial i}{\partial x} \tag{38}$$

The reference point for the electric potential is set *inside* the lithium anode, allowing for simple calculation of the potential *outside* but next to the anode as a Dirichlet boundary condition, denoted by $\phi_A$. The anode has an equilibrium potential difference with respect to the electrolyte $\Delta\phi_{eq,A}$ given by the Nernst equation:

$$\Delta\phi_{eq,A} = V^0 + \frac{k_B T}{ne}\ln\left(\frac{c}{N_A \cdot 10^3}\right) \tag{39}$$

Here $V^0$ is the standard electrode potential valued at $3.04V$ for lithium metal. Again $n$ is the number of moles of electrons that react per mole lithium, which is 1. $N_A \cdot 10^3$ is the conversion factor from number concentration per $\mathrm{m}^3$ to mole per liter. The overpotential at the anode $\eta_A$ is constant with a CC model. $\phi_A$ differs from reference (zero) by the sum of the overpotential

and the equilibrium potential difference:

$$\phi_A = \Delta\phi_{eq,A} + \eta_A \tag{40}$$

On the right the potential has a zero Neumann boundary condition, which can be understood from the fact that the electric field in the electrolyte vanishes at the right current collector, at this location all charge transport takes place in the form of electrons entering the solid matrix.

Equation T1.3 is only used as a definition for the current, since that is an interesting variable of the battery. Before discretising the equations T1.3 will be substituted into T1.1. The boundary conditions are linked to T1.1, at the anode the CC value must enter the electrolyte, giving the value $\boldsymbol{i}|_{x=0} = I/A$. No exchange of lithium or electrons takes place and the cathode current collector, giving $\boldsymbol{i}|_{x=0} = 0$. There lithium is absorbed by the active particles, and electrons enter the cathode through the solid matrix, not through the electrolyte.

Solving for the reaction rate requires more intricate reasoning, and eventually solving a nonlinear system of $P$ equations where $P$ is the number of particles modeled. Let $i = 1, \ldots, P$ be the particle index. Separate instances of equations T1.4.1, T1.4.2, T1.4.3 and T1.5 exist for each particle. Because the particles are modeled at grid points, the reaction rate index corresponding to a particle is the analogue of the space discretisation $j_{in,i} = j_{in}(x_i)$. We have established that the current density into a modeled particle $j_{in,i}$ can be expressed in terms of the overpotential of the intercalation reaction using the Butler-Volmer equation T1.4.1. The overpotential is defined as the difference between the observed potential difference of the reaction at a certain current and the potential difference at equilibrium, equation T1.4.2. The equilibrium potential difference of a particle is defined by T1.4.3, and hence dependent on the lithium concentration in the particle $c_{s,i}$. There are two kinds of constraints on the set of variables, namely:

- The total current from to electrolyte to the cathode particles is equal to the current into the battery from the anode:
$$\sum_i V_i a_p j_{in,i} = I \tag{41}$$
- All the lithium atoms entering a cathode particle have during one time step traversed the same potential drop throughout the battery:
$$\phi_i + \Delta\phi_i + \eta_i = \phi_j + \Delta\phi_j + \eta_j \quad \forall i, j \tag{42}$$

Equation 41 is a charge conservation constraint. The electrolyte cannot store any significant net charge during a time step in the model, all charge entering (in the form of lithium) will have to leave the electrolyte in the same time step. While particle $i$ represents the reactivity of a volume, there is a large number of particles in this volume. Hence each current density $j_{in,i}$ is multiplied by the surface area of active particles per unit volume $a_p$ and the volume $V_i$ of the discretisation volume.
The actual potential drop throughout the battery is $(-\phi_A + \phi_i) + \Delta\phi_i + \eta_i$, the terms representing the drop in the electrolyte, the drop associated with the intercalation reaction and the overpotential for the reaction respectively. $\phi_A$ is left out since it is present for each particle. Equation 42 is intuitively related to the idea of the battery voltage. For a voltage to be defined at any point in time it cannot be the case that lithium atoms experience different total potential drops during their journey from anode to cathode. All atoms completing the journey in the same time step will in the end have traversed the same potential drop. The key is that the

distribution of the potential drop can vary. Suppose two particles have a different local electrolyte potential: $\phi_i > \phi_j$. Now lithium at $i$ has more of its potential left, and there could be a more negative overpotential at $i$, $\eta_i < \eta_j$, meaning a greater reaction rate at $i$. Since $\Delta\phi_{i,eq}$ is dependent on $c_{s,i}$, the state of charge of the particles will also influence the distribution of the potential drop. When a particle is nearly fully lithiated, $\Delta\phi_{eq,i}$ will become increasingly negative pushing the balance away from negative overpotentials, yielding the decreasing reaction rate expected from nearly full particles. $P-1$ instances of equation 42 exist, most conveniently obtained by using consecutive particles for $i$ and $j$, e.g. $i = 1, j = 2$ and $i = 2, j = 3$ and so forth.

Combining equations 41 and 42 the set of $P$ equations can be solved, obtaining the $P$ unknown overpotentials $\eta_i$, which simply give the reaction rates $j_{in,i}$ through the Butler-Volmer equation T1.4.1. Because T1.4.1 is non-linear it will be necessary to use a nonlinear iterative solving scheme.

The boundary conditions for T1.5 are straightforward again. Both are Neumann, the left corresponding to the outer edge of the particle, hence equal to the current density $j_{in}$, and the right being zero since it represents the center of the particle.

Substituting T1.3 into T1.1 leaves $c(x,t)$, $\phi(x,t)$ and $j_{in}(x,t)$ to be solved using two differential equations and a non-linear system. The adapted version of T1.1 is given by

$$\frac{\partial c}{\partial t} = (D_{amb} + (D_+ - D_-)t_+)\frac{\partial^2 c}{\partial x^2} - \frac{\partial}{\partial x}\left(\frac{\partial \phi}{\partial x}c\right) - \frac{a_p j_{in}}{\epsilon} \tag{43}$$

with the diffusion terms grouped together and a convection term with the gradient of $\phi$ as a variable coefficient. A time based convection-diffusion equation with a source term and $\phi$-dependent coefficients for the convection part.

### 3.2.2 Pseudocode

Figure 8 shows a global pseudocode overview of the code. After finding an equilibrium initial condition with no current flowing, the constant current demand will be quickly ramped up over a number of time steps. The segregated solution algorithm solves for the equations T1.1 up to T1.4 without changing the state of charge of the active particles. The reaction rates from the resulting equilibrium are used to update the state of charge of each particle by integrating the diffusion in time. The new states of charge are again fixed for the next iterations of the segregated solution algorithm. Below, the discretisation of the equations and stability criteria will be discussed.

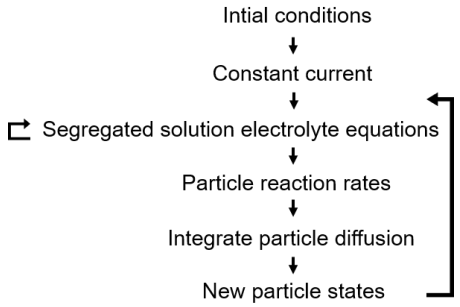


Figure 8: Order of computations in the model.

### 3.2.3 Nondimensionalisation

Without further treatment, the units of the equations in table 1 lead to values of some variables that are extremely large or small. By default the electrolyte concentration is in number concentration $\left[\frac{1}{m^3}\right]$, and its value is some orders of magnitude greater than the Avogadro number, $6.022 \cdot 10^{23}$. For the sake of computational stability it is important to change the set of equations such that the variables will have more manageable values (Smith & Bazant, 2017). This is done through nondimensionalisation. All dependent and independent variables are scaled by a characteristic value with the same unit. Let nondimensional variables be marked by a tilde. Nondimensional distance for example is given by $\tilde{x} = \frac{x}{x_{\text{ref}}}$, with $x_{\text{ref}}$ a characteristic length, in this case we use the cathode length $L_c$.
The procedure to nondimensionalise the system of equations starts by expressing all variables by their nondimensional counterpart and scale factor:

$$\begin{aligned} x &= \tilde{x}\, L_{\text{c}} \\ t &= \tilde{t}\, t_{\text{ref}} \\ c &= \tilde{c}\, c_{\text{ref}} \\ \phi &= \tilde{\phi}\, \phi_{\text{ref}} \\ \boldsymbol{i} &= \tilde{\boldsymbol{i}}\, \boldsymbol{i}_{\text{ref}} \\ j_{in} &= \tilde{j}_{in}\, j_{in_{\text{ref}}} \end{aligned} \tag{44}$$

and substituting these into the equations. For derivatives the relation

$$\frac{\partial}{\partial y} = \frac{1}{y_{\text{ref}}} \frac{\partial}{\partial \tilde{y}} \tag{45}$$

is used. We take the scale factors for the first three variables as $L_c$, $t_{ref} = L_c^2/D_{amb}$ and $c_{ref} = 10^3 \cdot N_A\ \text{m}^{-3} = 1\text{M}$, and then divide through by the prefactor of the highest order derivative in T1.1. Now we can strategically set as many prefactors to 1 by choosing the lower three scale factors in 44. Following through this process with the other equations solves for all scale factors, resulting in the following:

$$\begin{aligned} \phi_{ref} &= \frac{k_B T (D_+ - D_-)}{e(z_+ D_+ - z_- D_-)} \\ \boldsymbol{i}_{ref} &= \frac{e D_{amp} N_A}{\text{t}_+} \\ j_{in_{ref}} &= \frac{D_{amp} N_A}{a_p} \end{aligned} \tag{46}$$

After nondimensionalisation, the largest order of magnitude in the nondimensional variables is $10^4$, and all prefactors are at worst of the same order of magnitude as 1. Because the units $\text{A/m}^2$ and $V$ of $e\, j_{in}$, $\eta$ and $\Delta\phi$ will result in values relatively close to 1 the system T2.3 is kept dimensional. Simple multiplication and division by $e\, j_{in_{\text{ref}}}$ will suffice for switching to and from $\tilde{j}_{in}$. Table 2 gives the set of equations in terms of the nondimensional variables.

Table 2: Set of nondimensional equations

| # | Dependent variable | Equation | Boundary conditions |
|---|---|---|---|
| (T2.1) | Concentration $\tilde{c}$ | $\frac{\partial \tilde{c}}{\partial \tilde{t}} = \left(\frac{D_{amb}+(D_+-D_-)t_+}{D_{amb}}\right)\frac{\partial^2 \tilde{c}}{\partial \tilde{x}^2} - \frac{t_+(D_+-D_-)}{D_{amb}}\frac{\partial}{\partial \tilde{x}}\left(\frac{\partial \tilde{\phi}}{\partial \tilde{x}}\tilde{c}\right) - \frac{L_c^2 \tilde{j}_{in}}{\epsilon}$ | $\frac{\partial \tilde{c}}{\partial \tilde{x}}\vert_{\tilde{x}=0} = \frac{IL_c}{AD_+c_{\text{ref}}}$<br>$\frac{\partial \tilde{c}}{\partial \tilde{x}}\vert_{\tilde{x}=L/L_c} = 0$ |
| (T2.2) | Electric potential $\tilde{\phi}$ | $\frac{L_c D_{amb}}{\epsilon(D_+-D_-)}\tilde{j}_{in} = \frac{\partial^2 \tilde{c}}{\partial \tilde{x}^2} + \frac{\partial}{\partial \tilde{x}}\left(\tilde{c}\frac{\partial \tilde{\phi}}{\partial \tilde{x}}\right)$ | $\tilde{\phi}\vert_{\tilde{x}=0} = \phi_A/\phi_{\text{ref}}$<br>$\frac{\partial \tilde{\phi}}{\partial \tilde{x}}\vert_{\tilde{x}=L/L_c} = 0$ |
| (T2.3.1) | Reaction rate $j_{in,i}$ | $e\ j_{in,i} = \boldsymbol{i}_0\left[exp\left(-\frac{\alpha e \eta_i}{k_B T}\right) - exp\left(\frac{(1-\alpha)e\eta_i}{k_B T}\right)\right]$ | $\sum_i V_i a_p j_{in,i} = I$ |
| (T2.3.2) | - | $\eta_i = \Delta\phi_i - \Delta\phi_{eq,i}$ | $\phi_i + \Delta\phi_i + \eta_i = \phi_j + \Delta\phi_j + \eta_j \quad \forall i,j$ |
| (T2.3.3) | - | $\Delta\phi_{eq,i} = V^0 - \frac{k_B T}{e}\ln\left(\frac{\tilde{c}_{s,i}}{1-\tilde{c}_{s,i}}\right) - \frac{\Omega}{e}(1-\tilde{c}_{s,i})$ | - |
| (T2.4) | Active particle concentration $c_{s,i}$ | $\frac{\partial c_s}{\partial t} = \frac{\partial}{\partial r}\left(D_{chem,s}\frac{\partial c_s}{\partial r}\right)$ | $\frac{\partial c_{s,i}}{\partial r}\vert_{r=0} = j_{in,i}$<br>$\frac{\partial c_{s,i}}{\partial r}\vert_{r=R} = 0$ |

### 3.2.4 Discretisation

Now the discretisation of equations T2.1 and T2.2 will be described. T2.1 is a time based convection-diffusion equation for $\tilde{c}$ with a $\tilde{j}_{in}$ source term and $\phi$-dependent variable coefficients for the convection term. T2.2 is a diffusion equation for $\tilde{\phi}$ with $\tilde{c}$ as a variable diffusion coefficient and source terms dependent on $\tilde{j}_{in}$ and $\tilde{c}$. A finite volume method would be suitable for discretising these equations, with the advantages of supporting variable grid sizes, and simply accommodating the Neumann boundary conditions. Still, the finite difference method was chosen for the final version of the model to circumvent having to use midpoint integration approximations for the terms without derivatives, and having to use averaging to approximate functions between nodes.

The domain is one-dimensional of length $L = L_e + L_c$, where $L_e$ is the separator length and $L_c$ is the cathode length. Let $N+1$ points denoted $x_0, \ldots, x_N$ be evenly spaced on the domain, with $x_i = ih$ where $h = \frac{L}{N}$ is the grid size. The finite difference scheme requires an equidistant grid, so for simplicity $h$ must be chosen such that $L_e$ and $L_c$ are both multiples of $h$. Time will be discretised by $T$ points of length $\Delta t$. To keep the notation compact we use $\tilde{c}_i^j = \tilde{c}(x_i, t_j)$. The derivatives are taken with respect to the nondimensional independent variables defined by $\tilde{h} = \frac{h}{L_c}$ and $\Delta\tilde{t} = \frac{\Delta t}{t_{\text{ref}}}$. This means dividing by the nondimensional grid size in finite differences formula, for example the central difference second derivative:

$$\frac{\partial^2 \tilde{c}_i^j}{\partial \tilde{x}^2} = \frac{\tilde{c}_{i-1}^j - \tilde{c}_i^j + \tilde{c}_{i+1}^j}{\tilde{h}^2} + \mathcal{O}(\tilde{h}^2) \tag{47}$$

For the diffusion term in T2.1 the error in equation 47 is neglected. For the boundary

conditions central differences with virtual points are used, namely:

$$\begin{aligned} \frac{\tilde{c}_1^j - \tilde{c}_{-1}^j}{2\tilde{h}} &= \frac{IL_\mathrm{c}}{AD_+ c_\mathrm{ref}} \quad \text{gives} \quad \tilde{c}_{-1}^j = \tilde{c}_1^j - 2\tilde{h}\frac{IL_\mathrm{c}}{AD_+ c_\mathrm{ref}} \\ \frac{\tilde{c}_{N+1}^j - \tilde{c}_{N-1}^j}{2\tilde{h}} &= 0 \quad \text{gives} \quad \tilde{c}_{N+1}^j = \tilde{c}_{N-1}^j \end{aligned} \tag{48}$$

Unfortunately the symmetry of the matrix $\boldsymbol{D}$ is lost with these boundary conditions. It will however not make a difference for the final system of equations, as $C^1$ will also become asymmetric when the gradient of $\tilde{\phi}$ is varying. The matrix $\boldsymbol{D}$ is shown below.

$$\boldsymbol{D} = \frac{D_{amb} + (D_+ - D_-)t_+}{D_{amb}\ \tilde{h}^2} \begin{bmatrix} -2 & 2 & 0 & & 0 \\ 1 & -2 & 1 & & \\ & \ddots & \ddots & \ddots & \\ & & 1 & -2 & 1 \\ 0 & & 0 & 2 & -2 \end{bmatrix} \tag{49}$$

The left hand boundary condition is nonhomogeneous and its value is incorporated in the vector $\boldsymbol{d}_\mathrm{BC}$, given by:

$$\boldsymbol{d}_\mathrm{BC} = \begin{bmatrix} -\frac{2}{\tilde{h}}\frac{IL_\mathrm{c}}{AD_+ c_\mathrm{ref}} \\ 0 \\ \vdots \\ 0 \end{bmatrix} \tag{50}$$

The convection term has the gradient of $\tilde{\phi}$ as variable coefficient function. It was decided to discretise this using secondary central differences for $\tilde{\phi}$ embedded into a primary central difference formula for $\tilde{c}$. Neglecting the error the finite difference formula 51 is obtained

$$\frac{\partial}{\partial \tilde{x}}\left(\frac{\partial \tilde{\phi}}{\partial \tilde{x}}\tilde{c}\right)(x_i, t_j) = \frac{\frac{\tilde{\phi}_{i+2}^j - \tilde{\phi}_i^j}{2\tilde{h}}\tilde{c}_{i+1}^j - \frac{\tilde{\phi}_i^j - \tilde{\phi}_{i-2}^j}{2\tilde{h}}\tilde{c}_{i+1}^j}{2\tilde{h}} \tag{51}$$

Using the above formula presents a difficulty for the terms near the boundaries, involving $\tilde{x}_{-1}$, $\tilde{x}_0$ and $\tilde{x}_{N+1}$. The gradient of $\phi$ or alternatively the electric field is unknown at these points. For $\tilde{x}_{N+1}$ outside the domain we can extend the condition of zero electric field at $\tilde{x}_N$. For $\tilde{x}_0$ there is no such condition, because the potential itself, not its gradient is fixed there. We reason that, because all the lithium entering the domain is already represented in the diffusion boundary condition, it is inconsistent to have the convection term cause a net lithium gain. Therefore $\frac{\tilde{\phi}_0^j - \tilde{\phi}_{-2}^j}{2\tilde{h}}$ and $\frac{\tilde{\phi}_1^j - \tilde{\phi}_{-1}^j}{2\tilde{h}}$ are also set to zero. The resulting convection matrix $\boldsymbol{C}^j$ is:

$$\boldsymbol{C}^j = \frac{(D_+ - D_-)t_+}{D_{amb}}\frac{1}{4\tilde{h}^2} \begin{bmatrix} 0 & \tilde{\phi}_2^j - \tilde{\phi}_0^j & 0 & & & \emptyset \\ 0 & 0 & \tilde{\phi}_3^j - \tilde{\phi}_1^j & 0 & & \\ 0 & \tilde{\phi}_2^j - \tilde{\phi}_0^j & 0 & \tilde{\phi}_4^j - \tilde{\phi}_2^j & & \\ & \ddots & & \ddots & \ddots & \\ & & \tilde{\phi}_{N-2}^j - \tilde{\phi}_{N-4}^j & 0 & \tilde{\phi}_N^j - \tilde{\phi}_{N-2}^j & 0 \\ & & & \tilde{\phi}_{N-1}^j - \tilde{\phi}_{N-3}^j & 0 & 0 \\ \emptyset & & & 0 & \tilde{\phi}_N^j - \tilde{\phi}_{N-2}^j & 0 \end{bmatrix} \tag{52}$$

Finally, rearranging gives the matrix vector equation used to solve the system.

$$\tilde{\boldsymbol{c}}^{j+1} = (\boldsymbol{I} - \Delta\tilde{t}(\boldsymbol{D} + \boldsymbol{C}^j))^{-1}(\tilde{\boldsymbol{c}}^j + \Delta\tilde{t}(\boldsymbol{d}_{\mathrm{BC}} - \frac{L_c^2 \boldsymbol{j}_{in}^j}{\epsilon})) \tag{53}$$

The system of equations for T2.2 contains one equation less than the system for T2.1, because $\phi$ has one Dirichlet boundary condition. Apart from that change and the resulting different first row the second derivative matrix $\boldsymbol{A}$ for $\tilde{c}$ is similar to $\boldsymbol{D}$:

$$\boldsymbol{A} = \frac{1}{\tilde{h}^2}\begin{bmatrix} -2 & 1 & 0 & \dots & 0 \\ 1 & -2 & 1 & & \vdots \\ \vdots & \ddots & \ddots & \ddots & \vdots \\ \vdots & & 1 & -2 & 1 \\ 0 & \dots & 0 & 2 & -2 \end{bmatrix} \tag{54}$$

The value $\tilde{c}_0^j/\tilde{h}^2$ is accounted for by the vector $\boldsymbol{a}_{\mathrm{BC}}^j$

$$\boldsymbol{a}_{\mathrm{BC}}^j = \begin{bmatrix} \frac{\tilde{c}_0^j}{\tilde{h}^2} \\ 0 \\ \vdots \\ 0 \end{bmatrix} \tag{55}$$

The term $\frac{\partial}{\partial\tilde{x}}\left(\tilde{c}\frac{\partial\tilde{\phi}}{\partial\tilde{x}}\right)$ represents a Laplace's operator weighted by $\tilde{c}$. Repeated central differences are the preferred option here, because this ensures a second order approximation (Kan, 2019). We take the central difference of $\tilde{c}\frac{\partial\tilde{\phi}}{\partial\tilde{x}}$ between two midpoints defined as $\tilde{x}_{i\pm\frac{1}{2}} = \tilde{x}_i \pm \frac{\tilde{h}}{2}$:

$$\frac{\partial}{\partial\tilde{x}}\left(\tilde{c}\frac{\partial\tilde{\phi}}{\partial\tilde{x}}\right)\Bigg|_{\tilde{x}_i}^{\tilde{t}_j} = \frac{c_{i+\frac{1}{2}}^j \frac{\partial\tilde{\phi}}{\partial\tilde{x}}(\tilde{x}_{i+\frac{1}{2}}, t_j) - \tilde{c}_{i-\frac{1}{2}}^j \frac{\partial\tilde{\phi}}{\partial\tilde{x}}(\tilde{x}_{i-\frac{1}{2}}, t_j)}{\tilde{h}} \tag{56}$$

Now $\frac{\partial\tilde{\phi}}{\partial\tilde{x}}$ is discretised using central differences, giving:

$$\frac{\partial}{\partial\tilde{x}}\left(\tilde{c}\frac{\partial\tilde{\phi}}{\partial\tilde{x}}\right)\Bigg|_{\tilde{x}_i}^{t_j} = \frac{\tilde{c}_{i+\frac{1}{2}}^j \frac{\tilde{\phi}_{i+1}^j - \tilde{\phi}_i^j}{\tilde{h}}(\tilde{x}_{i+\frac{1}{2}}, t_j) - \tilde{c}_{i-\frac{1}{2}}^j \frac{\tilde{\phi}_i^j - \tilde{\phi}_{i-1}^j}{\tilde{h}}(\tilde{x}_{i-\frac{1}{2}}, t_j)}{\tilde{h}} \tag{57}$$

The terms $\tilde{c}_{i\pm\frac{1}{2}}^j$ are approximated by the mean of their adjacent grid points, such that $\tilde{c}_{i+\frac{1}{2}}^j \approx k_{i+1}^j = \frac{\tilde{c}_{i+1}^j + \tilde{c}_i^j}{2}$. The final discretisation formula is given by

$$\frac{\partial}{\partial\tilde{x}}\left(\tilde{c}\frac{\partial\tilde{\phi}}{\partial\tilde{x}}\right)\Bigg|_{\tilde{x}_i}^{t_j} = \frac{k_{i+1}^j\tilde{\phi}_{i+1}^j - (k_{i+1}^j + k_i^j)\tilde{\phi}_i^j + k_{i-1}^j\tilde{\phi}_{i-1}^j}{\tilde{h}^2} \tag{58}$$

The equations are collected into the matrix $\boldsymbol{B}$:

$$\boldsymbol{B}^j = \frac{1}{\tilde{h}^2}\begin{bmatrix} -(k_2^j+k_1^j) & k_2^j & 0 & \dots & \emptyset \\ k_1^j & -(k_3^j+k_2^j) & k_3^j & & \\ 0 & k_2^j & -(k_4^j+k_3^j) & k_3^j & \vdots \\ & \ddots & \ddots & \ddots & \\ \vdots & & k_{N-2}^j & -(k_{N-1}^j+k_{N-2}^j) & k_{N-1}^j & 0 \\ & & & k_{N-1}^j & -(k_N^j+k_{N-1}^j) & k_N^j \\ \emptyset & \dots & & 0 & k_N^j+k_{N+1}^j & -(k_N^j+k_{N+1}^j) \end{bmatrix} \tag{59}$$

Here $\tilde{c}_{N+1}^j$ outside the domain was taken equal to $\tilde{c}_N^j$ because of the zero Neumann boundary condition at $\tilde{x}_N$, leading to $k_{N+1}^j = \tilde{c}_N^j$. The Dirichlet left boundary condition is taken into the vector $\boldsymbol{b}_{\mathrm{BC}}$ as follows:

$$\boldsymbol{b}_{\mathrm{BC}}\begin{bmatrix} \frac{\phi_a}{\phi_{\mathrm{ref}}}\frac{\tilde{c}_0^j+\tilde{c}_1^j}{2\tilde{h}^2} \\ 0 \\ \vdots \\ 0 \end{bmatrix} \tag{60}$$

Finally the source terms $\boldsymbol{A}\tilde{\boldsymbol{c}}^j$ and $\tilde{\boldsymbol{j}}_{in}^j$ are grouped together with the boundary condition vectors and the system is solved through taking the inverse of $\boldsymbol{B}^j$.

$$\tilde{\boldsymbol{\phi}}^j = \boldsymbol{B}^{-1}\left(-\boldsymbol{A}\tilde{\boldsymbol{c}}^j + \frac{L_c D_{amb}}{e(D_+ - D_-)}\tilde{\boldsymbol{j}}_{in}^j - \boldsymbol{a}_{\mathrm{BC}}^j - \boldsymbol{b}_{\mathrm{BC}}\right) \tag{61}$$

### 3.2.5 Nonlinear solver for T2.3

The exponential relation between the overpotential and the reaction rate calls for a non-linear solution algorithm for the system of equations T2.3 described above. The Newton-Raphson method uses the linear approximation of a function $f$ around an initial guess $x^0$ to calculate the intersection with the $x$-axis of this tangent function, namely $(x^1, 0)$. Next, $x^1$ is taken as the centerpoint for the linearisation of $f$, yielding a new point of intersection with the $x$-axis. This procedure can be extended to vector functions to solve systems of equations. In this case we want to know the $P$ overpotentials $\boldsymbol{\eta}$ that solve the system:

$$\boldsymbol{F}(\boldsymbol{\eta}) = 0 \tag{62}$$

where $f_1$ through $f_{(P-1)}$ are given by

$$f_i(\eta_i, \eta_{i+1}) = \phi(x_i) - \phi(x_{i+1}) + \Delta\phi_{eq,i} - \Delta\phi_{eq,i+1} + \eta_i - \eta_{i+1} = 0 \tag{63}$$

and $f_P$, the only nonlinear equation is given by

$$f_P(\boldsymbol{\eta}) = \frac{L_c a_p}{\epsilon}\sum_i \boldsymbol{i}_0\left[exp\left(-\frac{\alpha e\eta_i}{k_B T}\right) - exp\left(\frac{(1-\alpha)e\eta_i}{k_B T}\right)\right] - \boldsymbol{i}_{\mathrm{cell}} = 0 \tag{64}$$

We use a Taylor expansion around an initial guess vector of $\boldsymbol{\eta}^0$ on each equation, neglecting second order terms:

$$0 = \boldsymbol{F}(\boldsymbol{\eta}^0) + \boldsymbol{F}'(\boldsymbol{\eta}^0)(\boldsymbol{\eta}^1 - \boldsymbol{\eta}^0) \tag{65}$$

Where $\boldsymbol{F'}(\boldsymbol{\eta})$ is the Jacobian matrix at $\boldsymbol{\eta}$, in this case given by

$$\boldsymbol{F'}(\boldsymbol{\eta}) = \begin{bmatrix} \frac{\partial f_1}{\partial \eta_1} & \frac{\partial f_1}{\partial \eta_2} & \cdots & \frac{\partial f_P}{\partial \eta_1} \\ \frac{\partial f_2}{\partial \eta_1} & \frac{\partial f_2}{\partial \eta_2} & \cdots & \vdots \\ \vdots & & & \vdots \\ \frac{\partial f_P}{\partial \eta_1} & \cdots & \cdots & \frac{\partial f_P}{\partial \eta_P} \end{bmatrix} = \begin{bmatrix} 1 & -1 & 0 & \cdots & \cdots & 0 \\ 0 & 1 & -1 & \cdots & \cdots & 0 \\ \vdots & & \ddots & \ddots & & \\ \vdots & & & \ddots & \ddots & \\ \vdots & & & & 1 & -1 \\ \frac{\partial f_P}{\partial \eta_1} & \cdots & \cdots & \cdots & \cdots & \frac{\partial f_P}{\partial \eta_P} \end{bmatrix} \tag{66}$$

With the derivatives of $f_N$ given by

$$\frac{\partial f_P}{\partial \eta_i} = -\frac{L_c a_p}{\epsilon} \boldsymbol{i}_0 \left[ \frac{\alpha e}{k_B T} exp\left( -\frac{\alpha e \eta_i}{k_B T} \right) - \frac{(1-\alpha)e}{k_B T} exp\left( \frac{(1-\alpha) e \eta_i}{k_B T} \right) \right] \tag{67}$$

With $k$ the iteration number, the program constructs the matrix $\boldsymbol{F'}(\boldsymbol{\eta^k})$ and the vector $\boldsymbol{F}(\boldsymbol{\eta^k})$ and solves the system

$$\boldsymbol{F'}(\boldsymbol{\eta}^k)\boldsymbol{c}^k = -\boldsymbol{F}(\boldsymbol{\eta}^k) \tag{68}$$

Because $\boldsymbol{c^k} = (\boldsymbol{\eta}^{k+1} - \boldsymbol{\eta}^k)$ we find the next $\boldsymbol{\eta}^{k+1}$ by adding $\boldsymbol{c}^k$ and $\boldsymbol{\eta}^k$. The program continues until $||\boldsymbol{F}(\boldsymbol{\eta}^k)||$ is below a tolerance of $10^{-6}$.

### 3.2.6 Active particles

The active particle equation is a nonlinear diffusion equation. We discretise it using a finite volume method, and integrate with a forward Euler scheme. The particle length $R$ is the volume length. Let there be $N_p + 1$ nodes, denoted $r_0, \ldots, r_{N_p}$. The grid step lengths are given by $h_{p,k} = r_k - r_{k-1}$. We integrate equation T2.4 around an interior node $r_i$:

$$\int_{r_{i-\frac{1}{2}}}^{r_{i+\frac{1}{2}}} \frac{\partial c_s}{\partial t} dr = \int_{r_{i-\frac{1}{2}}}^{r_{i+\frac{1}{2}}} \frac{\partial}{\partial r} \left( D_{s,chem} \frac{\partial c_s}{\partial r} \right) dr \tag{69}$$

and hence

$$\frac{\partial}{\partial t} \int_{r_{i-\frac{1}{2}}}^{r_{i+\frac{1}{2}}} c_s dr = \left( D_{chem,s} \frac{\partial c_s}{\partial r} \right) \Bigg|_{r_{i+\frac{1}{2}}} - \left( D_{chem,s} \frac{\partial c_s}{\partial r} \right) \Bigg|_{r_{i-\frac{1}{2}}} \tag{70}$$

The derivatives $\frac{\partial c_s}{\partial r}$ are discretised with central differences. The variable diffusion coefficients are discretised by their average for the two neighbouring nodes. The lefthand integral is approximated using midpoint integration. Using $i$ for the spatial index, this results in:

$$\begin{aligned} \frac{\partial}{\partial t} \frac{1}{2} (h_{p,k} + h_{p,k+1}) c_{s,i} = & \left( \frac{D_{chem,s,i+1} + D_{chem,s,i}}{2} \right) \left( \frac{c_{s,i+1} - c_{s,i}}{h_{p,i+1}} \right) \\ & - \left( \frac{D_{chem,s,i} + D_{chem,s,i-1}}{2} \right) \left( \frac{c_{s,i} - c_{s,i-1}}{h_{p,i}} \right) \end{aligned} \tag{71}$$

For the boundary conditions a similar procedure is carried out, only the integration is taken over a half a volume, from $r_0$ to $r_{\frac{1}{2}}$ for the left boundary and from $r_{N_p - \frac{1}{2}}$ to $r_{N_p}$ for the right

boundary. Midpoint integration is replaced by one-sided integration. The derivatives evaluated on $r_0$ and $r_{N_p}$ are replaced by the Neumann boundary conditions. The resulting equations are:

$$\begin{aligned}\frac{\partial}{\partial t}\frac{1}{2}h_{p,1}c_{s,0} &= \left(\frac{D_{chem,s,1}+D_{chem,s,0}}{2}\right)\left(\frac{c_{s,1}-c_{s,0}}{h_{p,1}}\right)+D_{chem,s,0}\ j_{in}\\ \frac{\partial}{\partial t}\frac{1}{2}h_{p,N_p}c_{s,N_p} &= -\left(\frac{D_{chem,s,N_p}+D_{chem,s,N_p-1}}{2}\right)\left(\frac{c_{s,N_p}-c_{s,N_p-1}}{h_{p,N_p}}\right)\end{aligned} \tag{72}$$

Now we can define matrices of the system of equations 71 and 72. The left hand sides become the mass matrix:

$$\boldsymbol{M} = \frac{1}{2}\begin{bmatrix} h_{p,1} & & & & \emptyset \\ & (h_{p,1}+h_{p,2}) & & & \\ & & (h_{p,2}+h_{p,3}) & & \\ & & & \ddots & \\ & & & & (h_{p,N_p-1}+h_{p,N_p}) \\ \emptyset & & & & h_{p,N_p} \end{bmatrix} \tag{73}$$

The right hand sides become the matrix $\boldsymbol{L}$. Here the fraction $\frac{D_{chem,s,i+1}+D_{chem,s,i1}}{2}$ is abbreviated as $D_{i+\frac{1}{2}}$

$$\boldsymbol{L} = \frac{1}{2}\begin{bmatrix} -\frac{D_{\frac{1}{2}}}{h_{p,1}} & \frac{D_{\frac{1}{2}}}{h_{p,1}} & & & \emptyset \\ \frac{D_{\frac{1}{2}}}{h_{p,1}} & -\left(\frac{D_{1+\frac{1}{2}}}{h_{p,2}}+\frac{D_{\frac{1}{2}}}{h_{p,1}}\right) & \frac{D_{1+\frac{1}{2}}}{h_{p,2}} & & \\ & \ddots & \ddots & \ddots & \\ & & \frac{D_{N_p-1\frac{1}{2}}}{h_{p,N_p-1}} & -\left(\frac{D_{N_p-1\frac{1}{2}}}{h_{p,N_p-1}}+\frac{D_{N_p-\frac{1}{2}}}{h_{p,N_p}}\right) & \frac{D_{N_p-\frac{1}{2}}}{h_{p,N_p}} \\ \emptyset & & & \frac{D_{N_p-\frac{1}{2}}}{h_{p,N_p}} & -\frac{D_{N_p-\frac{1}{2}}}{h_{p,N_p}} \end{bmatrix} \tag{74}$$

The nonhomogeneous left hand boundary condition is represented by a vector $\boldsymbol{l}_{\mathrm{BC}}$:

$$\boldsymbol{l}_{\mathrm{BC}} = \begin{bmatrix} D_{chem,s,0}\ j_{in} \\ 0 \\ \vdots \\ 0 \end{bmatrix} \tag{75}$$

Finally the time derivative is approximated by using forward differences. The active particle model used a time step that is different from the electrolyte model, denoted $\Delta t_p$. Superscript $j$ is again taken as time index for the time dependent matrix and vectors. The solution in matrix-vector form:

$$\boldsymbol{c}_s^{j+1} = \boldsymbol{c}_s^j + \Delta t_p(\boldsymbol{M}^{-1}(\boldsymbol{L}^j + \boldsymbol{l}_{\mathrm{BC}}^j)) \tag{76}$$

### 3.2.7 Coupling and stability analysis

Coupling between the two volumes is achieved using $j_{in}$. The particles are modeled as cubes with edges of length $R$. Only two opposite faces of the particle are reactive surfaces (Bazant, 2012). So for a volume of $R^3$ the reactive surface be $2R^2$, so $a_p = \frac{2R^2}{R^3}$.
Equation T2.1 is integrated using an implicit backward Euler method for simplicity. The MPET model uses the implicit Crank-Nicolson scheme which has a smaller global error. Both methods are unconditionally stable. However, the relative dominance of migration transport in equation T2.1 affects the stability of the system. This dominance can be expressed by the Peclet number, defined as the ratio of advective transport due to the migration term and diffusive transport. $Pe > 1$ indicates advection is the dominant transport process. High Peclet numbers cause numerical oscillations in the solution, so it is important to verify that the Peclet number does not exceed 2. This is not expected in this application, the diffusive transport should stay dominant as long as the diffusivity is sufficient to satisfy the lithium transport demanded at a specified current. At high currents the limit of the diffusion transport will be reached, and advection will gain relative dominance. If the system needs to be solved at high Peclet numbers, upwind differencing will improve convergence at the cost of solution accuracy, so that is not preferred if it is not necessary (Kan, 2019).
The active particle model uses a forward Euler method because it is nonlinear. A backward Euler method would require solving a nonlinear system with Picard or Newton iterations. Implementing this would be one of the most fruitful improvements to the model, because $P$ instances of the active particle model are computed, making it certainly the most computationally intensive task. The stability condition for the Euler forward scheme is $\Delta t_p < \frac{h_p^2}{2D_0}$.

## 3.3 Interface Regions

The 1-D treatment of the electrolyte in the MPET model does not allow for explicit locality of active particles and their interface with the electrolyte. Hence, the MPET model uses the electroneutrality assumption:

$$\sum_i z_i c_i = 0 \qquad \text{everywhere} \tag{77}$$

The particles are in direct contact with the bulk electrolyte. This hinders the treatment of electrical double layers in the region near the boundaries of particles and the electrolyte. We will call this region the interface region. Solid electrolytes in particular show different behaviour near the particles than in a bulk electrolyte region. To incorporate electrical double layers and solid electrolyte effects in the MPET model to introduction of an additional finite-volume domain (interface region, IR) is proposed, that models the electrolyte at close range to the solid particles. The physics captured in this region include the diffuse double layer and possibly other phenomena. This alone could also be used without solid electrolyte modeling. The other two principal aspects to be considered when modeling solid electrolytes are:

- Adapting the Gibbs free energy functional to incorporate the stress and strain effects of cathode particles growing/shrinking in solid electrolyte, forming cracks for example.
- Reconsidering the use of Butler-Volmer reaction kinetics, because the contact between particles and grainy solid electrolyte is less efficient compared to liquid electrolyte.

A limitation of the general idea is that only a small number of particles per cathode volume are modeled, without mutual interaction. In the realistic mesostructure of a porous electrode a particle will certainly be influenced by its surroundings so this is a weakness, but having interface regions at all will likely still bring an overall improvement to the realism of the model. A visual representation of the idea is given in figure 10.

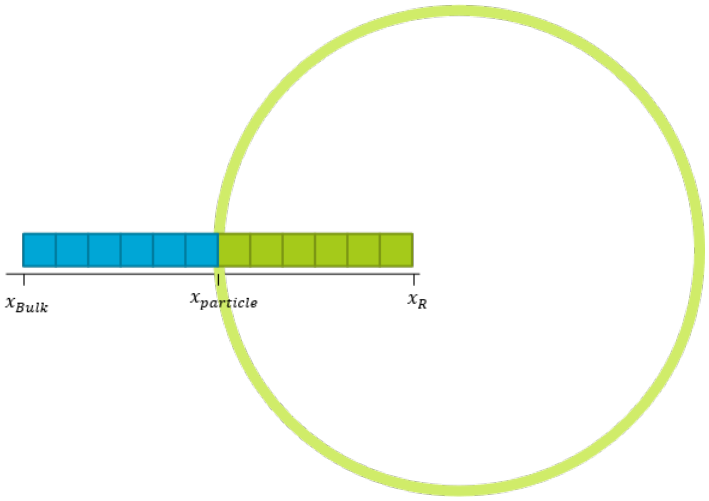


Figure 9: Visualisation of the model idea. $x_{bulk}$ and $x_{particle}$ are the boundaries for the interface region, the former coupled to the bulk electrolyte and the latter to the particle. $x_R$ is the end of the particle domain.

### 3.3.1 Double layers

To incorporate electrical double layers the electroneutrality assumption is dropped and the full Poisson-Nernst-Planck equations are solved in the interface region. This involves two mass conservation equations with concentrations $c_+$ (lithium) and $c_-$ (electrons) compared to the single mass conservation equation currently in the MPET model, and a Poisson-Boltzmann equation. First the electric potential is separated into the bulk electrolyte part and a contribution from the diffuse charge:

$$\phi = \bar{\varphi} + \varphi \tag{78}$$

with $\phi$ the total potential, $\bar{\varphi}$ the "bulk" potential and $\varphi$ the diffuse charge contribution. Knowing the value of $\bar{\varphi}$, it can be used as the reference in the IR, so that we only deal with $\varphi$ there. The boundary conditions for the potential will then be $\varphi(x = 0) = 0$ ($\phi = \bar{\varphi}$) and $\varphi(x = L) = \varphi_I$, with $\varphi_I$ the potential contribution at the interface.

$$\frac{\partial^2 \varphi_D}{\partial x^2} = -\frac{e(c_+ - c_-)}{\epsilon_0} \tag{79}$$

The mass conservation equations are

$$\epsilon \frac{dc_+}{dt} = D_+ \frac{\partial^2 c_+}{\partial x^2} + \frac{z_+ e c_+}{k_B T} \frac{\partial^2 \varphi_D}{\partial x^2} + r \tag{80}$$

$$\epsilon \frac{dc_-}{dt} = D_- \frac{\partial^2 c_-}{\partial x^2} + \frac{z_- e c_-}{k_B T} \frac{\partial^2 \varphi_D}{\partial x^2} + r \tag{81}$$

The mass conservation equations are equal in structure to the equation in the original model, but now the movement of lithium and electrons is separated. $r$ is the previously introduced weak solid electrolyte microstructure reaction term. In the interface region there is no sink term for the active particles anymore, interaction with the particles is handled through the boundary conditions.

#### Boundary conditions

At the $x_{bulk}$ boundary, we have:

$$\begin{aligned}
&\varphi_D = 0, \ (\phi = \bar{\varphi}) \\
&c_+ = c_- = c_{bulk} \quad \text{(there is electroneutrality at the bulk boundary, for continuity with the bulk model)} \\
&\frac{\partial c_+}{\partial x} = R_{V_i} \quad (R_{V_i} \text{ is the bulk sink term in volume } V_i)
\end{aligned} \tag{82}$$

On the $x_{particle}$ (right) side, we have

$$\begin{aligned}
&\frac{\partial \varphi_D}{\partial x} = \frac{q}{\epsilon_0} \quad (q \text{ is the surface charge density of the particle}) \\
&\frac{\partial c_+}{\partial x} = -j_{in} \quad \text{(Neumann boundary condition calculated using Butler-Volmer, or an alternative)} \\
&\frac{\partial c_+}{\partial x} = 0 \quad \text{(there are no electrons entering the particles)}
\end{aligned} \tag{83}$$

All equations can be nondimensionalised in the same way as the current equations in the MPET model.

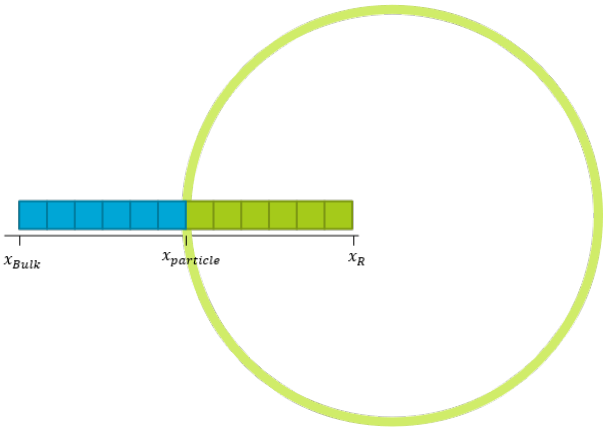


Figure 10: Visualisation of the model idea. $x_R$ is the end of the particle domain.

### 3.3.2 Stress effects

The active particles might display volume changes as they are (de)intercalating with lithium. For solid electrolytes this can form a problem because it the materials are rigid, not easily adapting to the active particles. Moreover, solid electrolytes generally perform better when packaged at high pressure, further decreasing the ability for solid particles to change volume. When the active particles do change volume, the electrolyte will face local pressures and stresses. The result of this can be that cracks form in the electrolyte, possibly reducing conductivity and stability of the material. When the electrolyte is a powder the conductivity can change due to these local changes in pressure and stresses, impacting diffusion through grain boundaries (Park, Zhang, Chung, Less, & Sastry, 2010). The strategy for modeling these effects is finding an appropriate expression for the change in Gibbs free energy of the system due to stress effects, $g_{stress}$. This is added to the totol Gibbs free energy:

$$g = g_{activity} + g_{electrostatic} + g_{stress} \tag{84}$$

We can calculate the electrochemical potential $\mu$ by taking a functional derivative of the Gibbs free energy. The the mass flux $F$, obtained from the electrochemical potential through $F = M_i c_i \nabla \mu$, can be working through into a new mass conservation equation with stress effects incorporated.

$$\epsilon \frac{dc}{dt} = -\nabla \cdot F \tag{85}$$

### 3.3.3 Reaction kinetics

The limitations of the Butler-Volmer equation to describe the reaction rate at the solid-solid interface between electrolyte and particle is frequently pointed out in literature (Kobayashi, Yamada, & Kanno, 2008). Specifically, the "wetting" of a surface by liquid electrolyte makes transfer of charged species easier because every irregularity on the particle surface is coated by electrolyte. With solid electrolyte this will not happen. The specific solid electrolyte used, and possible additive coatings all change behaviour, further complicating modeling. If a theory for this behaviour was developed it could be implemented in the interface region or the model.

# 4 Results and Discussion

First of all the correct behaviour of the original and changed models will be verified. This is done primarily by checking that the models obey mass conservation. Next, the performance of the glassy solid electrolyte model is compared to liquid electrolyte and another proposed solid electrolyte model by Landstorfer et al, see appendix B. Furthermore, the dependence of battery performance on the glassy electrolyte's equilibrium mobility fraction and recombination rate are studied. The role of solid electrolyte as a performance limiting part will also be studied. Next, the standalone model results will be discussed in section 4.2

## 4.1 MPET-model results

### 4.1.1 Verification of the model

Mass conservation is a fundamental assumption in the model, and thus it is important to check whether it is obeyed. Figure 11 shows the average lithium concentrations in the electrolyte during the full simulation time for liquid and solid electrolyte. Mass conservation states that these averages should stay constant. In all cases the concentration stays reasonably constant, within 2 percent of initial value. The liquid electrolyte model shows a sharp increase at the start of the simulation, likely due to the started procedure of the model. The current is ramped up quickly, and the particles do not respond before the average concentration has increased. The same likely occurs with the weak solid electrolyte model, yet in the concentration deviation it becomes relatively negligible because the solid electrolyte has a much greater concentration of host sites with lithium than the liquid electrolyte has of dissolved lithium. The general result is that apart from the initial ramping-up phase, mass conservation is adhered to.

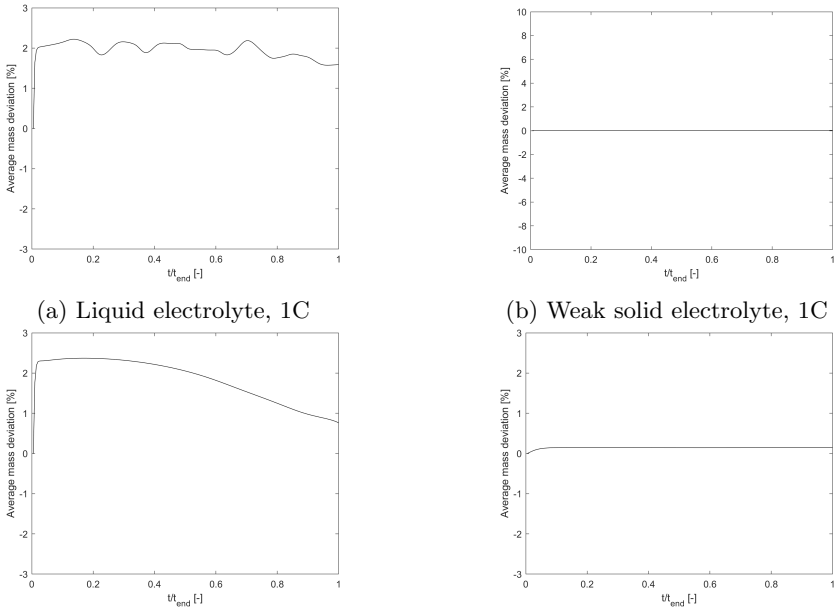


(a) Liquid electrolyte, 1C

(b) Weak solid electrolyte, 1C

(c) Liquid electrolyte, 5C

(d) Weak solid electrolyte, 5C

Figure 11: Comparison of the average concentration evolution for the liquid and weak solid electrolyte model.

### 4.1.2 Electrolyte models compared

In figure 12 the three electrolyte models are compared. The Landstorfer solid electrolyte model outperforms the other two models slightly in most runs, but the difference is small. The clear steps in voltage between the discharge rates are expected and a result of the activation overpotential at anode and cathode increasing with the discharge rate, causing effective voltage loss. Oscillations in the voltage occur at lower discharge rates, likely due to the cascading effect. Cascading refers to phase separating active particles at different locations lithiating fully in rapid succession but never together. When this happens there are significant local changes in electrolyte lithium concentration and potential, causing the oscillations in the battery voltage.
The effect of the cathode length starts to show at $1C$ and becomes pronounced at $5C$. In the longer cathode lithium depletion at the end of the cathode causes a decreasing voltage profile, because the lithium diffusion cannot keep pace with the lithiation. With a shorter cathode a voltage plateau is maintained. For battery design it is important to maximise cathode length for capacity while maintaining an acceptable voltage plateau. The difference in voltage between the weak solid electrolyte model and Landstorfer et al. model is consistent, hinting at an offset, possibly caused by an adaptation in the reaction kinetics formula used for the latter. In the $5C$ discharge for the $100\mu$m cathode the two solid electrolyte models differ from the liquid electrolyte in a similar way initially showing higher voltage but consistently dropping of immediately afterwards. Both models produce a performance penalty of the electrolyte at high concentrations. It can be explained by lithium concentration being high initially for the solid electrolytes, but diffusivity being significantly lower, the consequences of which become prevalent when discharging a long cathode at a fast rate.

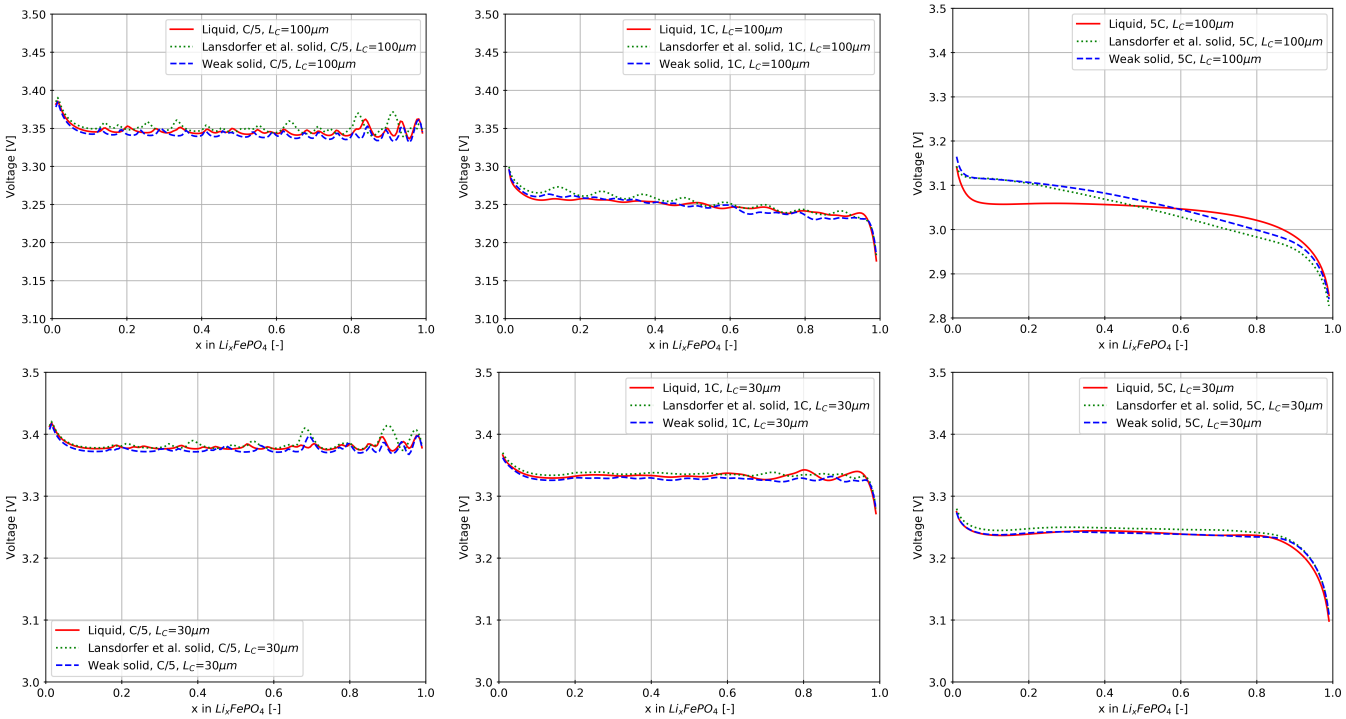


Figure 12: Comparison of the performance of the three electrolyte models across varying discharge rates. Top row: cathode length $L_c = 100\mu m$. Bottom row: $L_c = 30\mu m$.

### 4.1.3 $\delta$ and $k_r$ dependence

Figure 13 shows the weak solid electrolyte performance for a range if $\delta$ values. It is clear that lower equilibrium mobility fractions result in lower overall battery voltage, similar to how a overly dilute liquid electrolyte would limit performance. The effect is more severe for faster discharge rates, because in that case lithium cannot be transported to the active particles fast enough. At $C/5$ and $1C$ lower $\delta$ also results in smaller and less regular oscillations in the voltage profile. A possible reason for this is that the cascading effect is prevented. It would be prevented when lithium cannot be supplied to the single particle quickly enough for full lithiation to occur in a short amount of time.

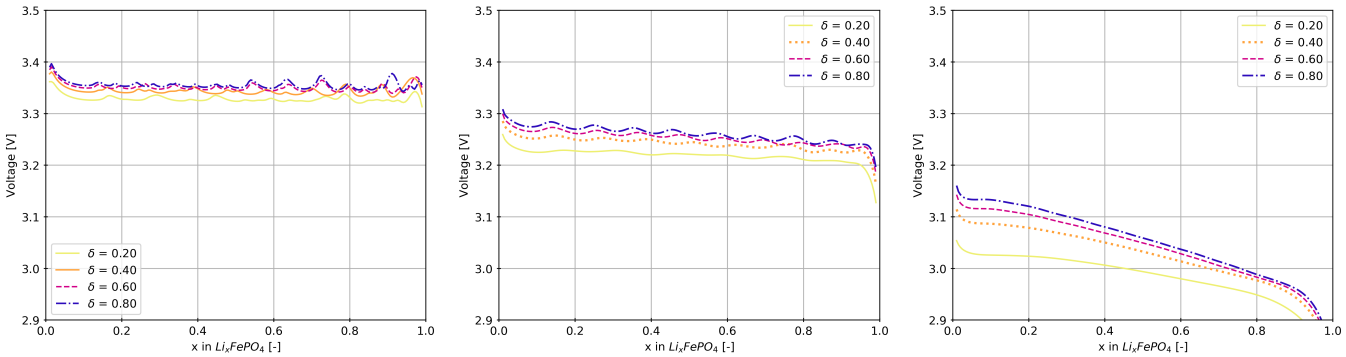


(a) C/5 (b) 1C (c) 5C

Figure 13: Comparison of the weak solid electrolyte model performance for a range of $\delta$ values.

The equilibrium mobility fraction is dependent on the activation energy of lithium in the material. This is not the activation energy generally described for diffusion in solids, but rather an activation energy for lithium to separate a host site and enter the interstitial phase. Materials with lower activation energies will have a higher interstitial lithium fraction, giving better performance.

In figure 14 the model's dependence in the recombination rate $k_r$ is plotted. The recombination rate appears to have minimal effect on performance, even though the range of discharge rates spans multiple orders of magnitude.

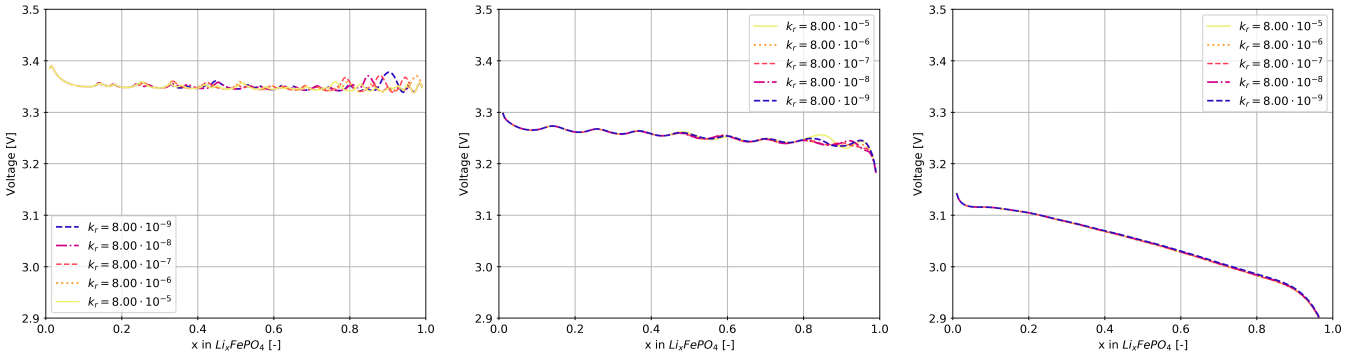


(a) C/5 (b) 1C (c) 5C

Figure 14: Comparison of the weak solid electrolyte model performance for a range of $k_r$ values.

At the low discharge rate in figure 14a, the voltage profile of the highest recombination rate $k_r = 8.00 \cdot 10^{-5}$ shows oscillations that are smaller but more frequent than for the other discharge rates. This is likely due to the relative insignificance of lithium depletion. When the recombination rate is lithium will enter the interstitial phase faster when a local deficiency occurs, effectively equalising the concentration across the electrolyte.

## 4.2 Standalone model results

The modeling method described in section 3 was found to yield a functioning and stable model. There are however some unexpected discrepancies between the electrolyte and active particle domains. In this section a run of the model will be studied to analyse the behaviour and compare it with what was expected.

The model run was performed at a discharge rate of $5C$, with 13 nodes in the electrolyte and 12 volumes in the active particles. 8 particles were simulated using a time step of $\Delta t_p = 0.01$ seconds. The 150 time steps used in the electrolyte give $\Delta t = 4.8$ seconds, so each completed electrolyte iteration was followed by 480 steps of active particle time integration at the found reaction rate. No solid electrolyte physics was implemented in this model, so the diffusion coefficients are taken to be the default values in MPET for liquid electrolytes. All the other relevant parameters are listed in appendix C.

Looking at the performance of the model, it is less efficient than the MPET model, taking around 5 minutes to complete a run at $5C$, which represents a full discharge in 12 minutes. The majority of that time is needed for integrating the active particle model. Changing the discharge current does not change the time step, so the slower the discharge current the more time the model will need integrating extra time steps. Also, because each grid point in the cathode requires modeling of at least one active particle, a fine grid in the electrolyte incurs a large performance penalty. Possible solutions for this are improving the stability criterion for the actively particle model allowing a greater time step, or alternatively using a single particle to represent the reaction rate at multiple electrolyte grid nodes. With the realism of the model in mind, the former would have preference, since roughly 10 particles is the minimum required to observe the behaviour caused by the depth of the cathode.

The voltage profile obtained by the run is shown in figure 15. It does not satisfy expectations, because the shape of the curve and its spread are what would be expected form the first phase of a discharge. A rapid voltage decrease is observed initially, after which the voltage plateau is gradually approached. Yet the model finished before the voltage plateau is reached. The particles have in fact not fully lithiated, as will be shown later. This is indicative of the discrepancy between the electrolyte and active particle domains. While both work as expected when isolated, the reaction rate found by the electrolyte model causes the active particles to lithiate too slowly.

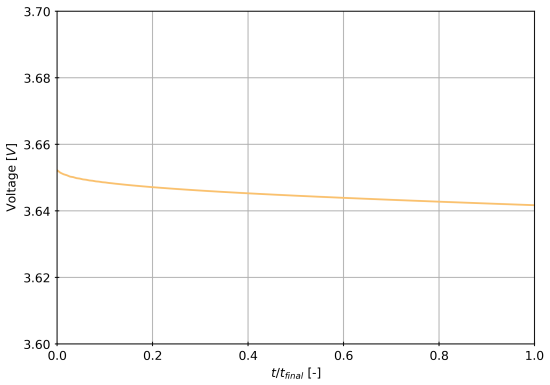


Figure 15: Voltage profile of a $5C$ run of the standalone model.

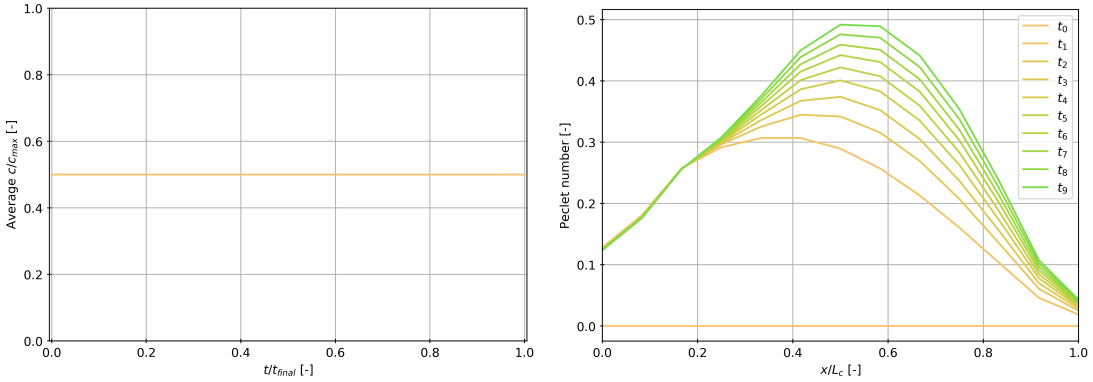


(a) Average lithium concentration in the electrolyte over time.

(b) Time evolution of the Peclet number in the electrolyte. $t_0$ is the initial condition and subsequent $t_i$ are evenly distributed.

Figure 16: Voltage and mass conservation for a $5C$ model run.

The constant average concentration in figure 16a shows that the electrolyte model wholly adheres to mass conservation. Figure 16b shows that the Peclet number does not surpass 0.5 during this run, staying well within the bound of $|Pe| < 2$. It is however steadily increasing, due to the increasing potential gradient. This is normal for the first stage of the model, when lithium is depleted near the end of the cathode. As lithiation progresses, the region of depletion will shift towards the left. The region with the greatest potential gradient will follow the lithium depletion, and because the potential gradient drives the migration (convection) term, the Peclet number will also be the greatest in this region. The argument made is that this is why even under normal behaviour, with the particles lithiating more quickly, the Peclet number will not increase significantly, only the peak of its distribution will be shifted along with the potential gradient. At higher currents the potential gradient will be greater, so that could become problematic for the Peclet number. However at high discharge rates over the MPET model can also have instabilities, so this would directly not disqualify the methodology of the standalone model.
In figure 17 the time evolution of the three electrolyte field variables and the concentration of one active particle are shown. Figure 17a shows the lithium-rich region near the anode and a lithium-poor region deep into the cathode, with the difference slowly increasing. The local electrolyte potential is highly dependent on the local lithium concentration, as expected. The slow particle lithiation is visible in figure 17d, which is only negligibly lithiated after completion of the model.
After initially being positive for all particles the reaction rate soon becomes negative for the first group of particles in the cathode. This is not expected and further highlights the problem with determining the reaction rates. At any stage in the model the charge conservation of equation 41 holds, restated here

$$\sum_i V_i a_p j_{in,i} = I \tag{86}$$

This is also a prerequisite for mass conservation. The problem can be split in two parts. Firstly the reaction rate is too low for the particles to lithiate significantly in each time step. This could be due to a fault in the expression of $V_i$, which was taken as $V_i = \frac{L_c(1-\epsilon)}{\#_{\text{cathode nodes}}}$, because the battery length represented by one node is the cathode length divided by the number of cathode nodes and only a fraction of $1-\epsilon$ is in fact active particle. The condition 86 formulated differently may result in a correct reaction rate. The second disparity is that the reaction rate becomes

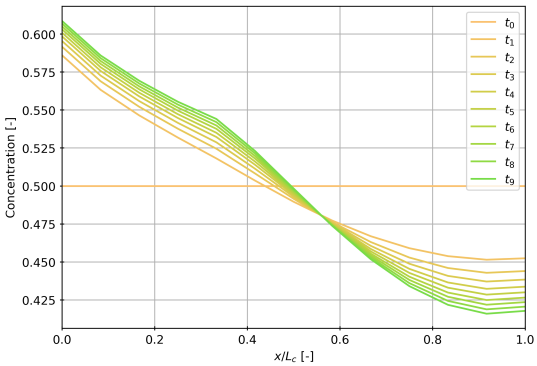


(a) Electrolyte potential compared to the reference, lithium metal.

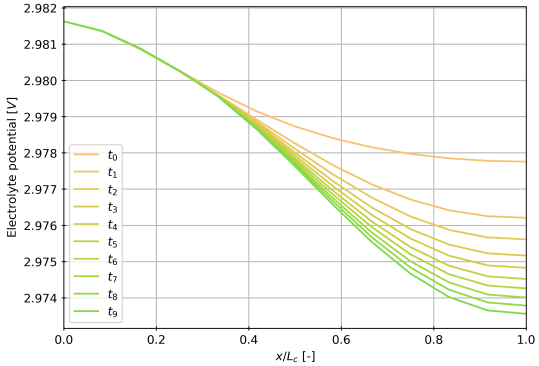


(b) Nondimensional electrolyte concentration.

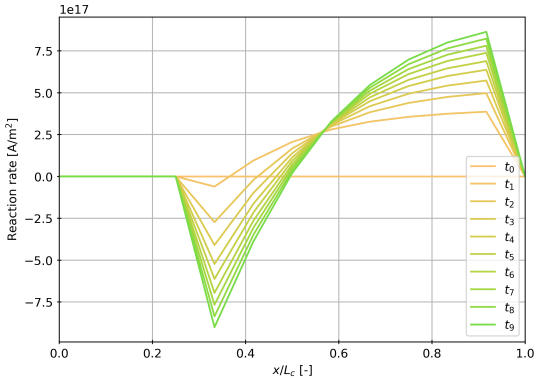


(c) Reaction rate distribution. Positive values indicate lithium being consumed by active particles.

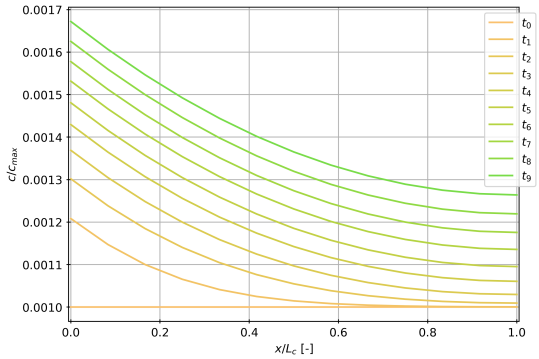


(d) Nondimensional concentration distribution of particle 7.

Figure 17: Summary of the model's field variables and particle 7 of eight positioned close to the current collector. $t_0$ is the initial situation with subsequent $t_i$ are evenly distributed.

negative in a region, even if the total reaction rate still ensures mass conservation. Changing 86 will amount to a different scaling of the reaction rate, but not eliminate the negative region. Possibly $a_p$ and the relationship between the particle length and the reactive area should be redefined.

All in all the model's two domains work properly in isolation, however a fault in the coupling between the domains cause the reaction rate to be too low and wrongly negative in a large region. Either there is a problem with the theoretical groundwork and the reasoning done there, or a crucial bug in the code.

### 4.2.1 Active particle model

With the active particles not lithiating quickly enough in the complete model, it remains of interest to inspect the lithiation behaviour when isolating the particle model. The expected phase separation when $\Omega > 2k_BT$ should be observed, and differences in intercalation rates will lead to different behaviour. Figure 18 shows a $FePO_4$ particle lithiating at three overpotentials and corresponding current densities, with the general solution parameter set to $\Omega = 3k_BT$. The duration of the lithiation simulated was 100 seconds.

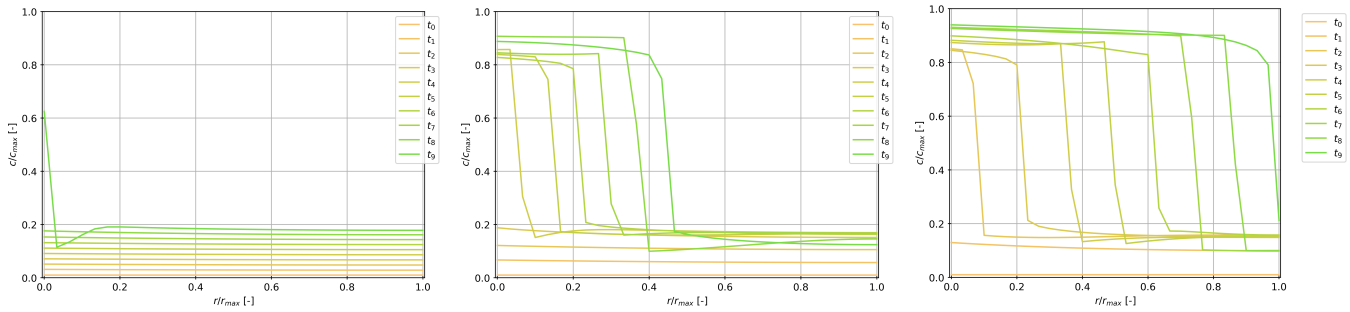


(a) Slow lithiation at an overpotential of $\eta = -0.01\ V$. The onset of phase separation is delayed.

(b) Half lithiation in one simulation, at an overpotential of $\eta = -0.025\ V$.

(c) Fast lithiation at an overpotential of $\eta = -0.045\ V$. Full lithiation is reached at the end of the simulation.

Figure 18: Comparison of three intercalation rates of a $FePO_4$ particle. The regular solution parameter is set to $3k_BT$. $t_0$ is the initial condition and the subsequent $t_i$ are evenly distributed.

Clear phase separation is visible in figures 18b and 18c. The phase boundary moves to the center of the particle as was predicted by the shrinking core model, see figure 7. At a slow lithiation speed shown in figure 18a the onset of phase separation is delayed, and a homogeneous increase in concentration is preferred by the model. The reason for this is that as long as all lithium can be stored without the concentration exceeding $\frac{c_s}{c_{s,max}} \approx 0.2$, phase separation is not preferred to minimise the free energy, since all lithium can be stored without anywhere leaving the lower minimum of free energy. As soon as more lithium is added the lower minimum have to be exceeded, making phase separation preferable. The start of this is shown by the green graph of figure 18a.

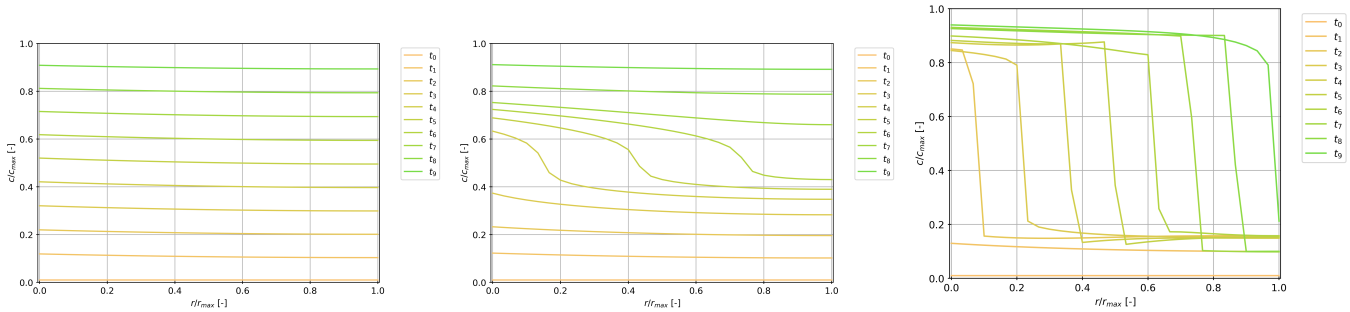


(a) $\Omega = 1k_BT$ (b) $\Omega = 2k_BT$ (c) $\Omega = 3k_BT$

Figure 19: The effect of the regular solution parameter on the phase separating behaviour of the active particles. $t_0$ is the initial situation with subsequent $t_i$ are evenly distributed.

The effect of the general solution parameter is shown in figure 19. The model correctly reproduces the expected dependence on $\Omega$, with phase separation at $\Omega = 3k_BT$ and homogeneous lithiation at $\Omega = 1k_BT$ Figure 19b shows the crossover case at $\Omega = 2k_BT$, where it is already visible that concentrations around $\frac{c_s}{c_{s,max}} \approx 0.5$ are not preferred as the concentration distribution nearly separates in two concentrations once it reaches halfway lithiated, and becomes homogeneous again once the halfway mark is passed.

# 5 Conclusions

Two solid electrolyte models were implemented into the MPET software. Adherence to mass conservation was verified successfully. There was a small consistent voltage difference between the two models, to the advantage of the Landstorfer et al. model. Aside from this, the models shows good agreement and differed from the liquid electrolyte model in similar ways. Primarily, the lower diffusivity of solid electrolytes does limit the performance of solid electrolytes in bulk-type batteries, as was visible even with the optimistic diffusivity values used. The solid electrolytes tend to cause more oscillation in the voltage profile, likely due to the lithium transport being limited by the lithium concentration. The equilibrium mobility fraction $\delta$ had significant effect on battery performance, indicating that materials with high $\delta$ and associated low activation energy for lithium to enter the interstitial phase are desirable properties for a solid electrolyte. The recombination rate $k_r$ shows less influence on performance, only slightly lowering oscillations in the voltage profile. It is important to verify the models results experimentally.
Of course, the main research effort into solid electrolytes is into improving lithium conduction of solid electrolytes. Apart from the diffusion mechanisms and the resulting behaviours, there are other factors of importance in the development of new solid electrolyte materials. Some can be modeled, such as the stability of the material under repeated charge cycling, response to deformations of the active material and the conduction through the boundary with the active particles. Experimental verification of theories enables fast comparisons of materials and proposed battery geometries using modelling. Others properties of the material are to be considered separately, such as the availability and sustainability of the materials, and simplicity and cost of production.

The standalone model has a fault at the coupling stage between the active particles and the electrolyte. Both domains work well in isolation but in a combined run the reaction rate is unrealistically low. If the standalone model were fully functional its many parameters would make it suitable to optimise for battery geometry and used materials. To this end there are several recommended expansions and improvements, some decidedly simple to implement. One of these expansions is allowing multiple particles with different sizes to be simulated at each node, which would improve realism. Additionally, spreading the reaction rate of such a set of particles across a region of nodes, would allow the electrolyte's spatial grid to be more fine without a large computational penalty. Of course, the solid electrolyte diffusion physics can be easily carried over from the MPET model. And lastly a backward integration for the active particle model with a nonlinear solver would improve computation times significantly.

For future research and expansion of the MPET model interface regions are an interesting option to pursue. The concept has its flaws, mainly the fact at each region only models the electrolyte near a single active particle, neglecting possible interactions when interface regions overlap. However, in essence it allows for the best of both Poisson-Nernst-Planck based models with rigorous treatment of boundary effects thanks to waiving the electroneutrality approximation, and porous electrode models that capture the behaviour of deep, high capacity electrodes. Solid electrolytes display more intricate effects such as dynamic stress and conduction through the boundary between solid electrolyte and active particle, which could likely all be incorporated in a model with interface regions.

# Appendices

## A Derivation of the solid particle model

We start with the mass flux given by concentrated solution theory:

$$\boldsymbol{F_i} = -M_i c_i \nabla \mu_i \tag{87}$$

where $M_i$ is the mobility of species $i$, $c_i$ is the concentration of species $i$ and $\mu_i$ is the chemical potential of species $i$. There are no sources or sinks in the active material, so the mass conservation equations becomes:

$$\frac{\partial c_s}{\partial t} = -\nabla \cdot \boldsymbol{F_s} \tag{88}$$

For the chemical potential we use the regular solution model. The regular solution model free energy is given by

$$g = k_B T[\tilde{c}_s \ln \tilde{c}_s + (1-\tilde{c}_s)\ln(1-\tilde{c}_s)] + \Omega \tilde{c}_s(1-\tilde{c}_s) \tag{89}$$

Where $\tilde{c}_s$ is the dimensionless solid concentration $\tilde{c}_s = c_s/c_{s,max}$. The rightmost term represents the 'entropy of mixing', and the regular solution parameter $\Omega$ is effect of the pairwise interaction of the intercalating species on the free energy. With this free energy model both homogeneous and phase-separating behaviour can be represented. When $\Omega < 2k_BT$ there is a single minimum in the free energy, resulting in homogeneous behaviour. If however $\Omega > 2k_BT$ there will to two minima leading to a phase boundary between these two concentrations. The chemical potential is given by:

$$\mu = \frac{\partial g}{\partial c_s} = k_B T \ln\left(\frac{\tilde{c}_s}{1-\tilde{c}_s}\right) + \Omega(1-2\tilde{c}_s) \tag{90}$$

To obtain a mass balance equation in a suitable form for numerical solving, equation 87 is written as

$$\boldsymbol{F}_s = -D_0(1-\tilde{c}_s)\left(1 + \frac{\partial \ln \gamma_s}{\partial \ln c_s}\right)\nabla c_s = -D_{chem}\nabla c_s \tag{91}$$

where $D_0$ is the diffusivity in the infinitely dilute limit. Using the definition of chemical potential, $\mu = k_B T \ln(c\gamma)$, and equating it to the chemical potential by the regular solution model 90, we can isolate $\ln\gamma_s$

$$\ln \gamma_s = \ln\left(\frac{\tilde{c}_s}{1-\tilde{c}_s}\right) + \frac{\Omega}{k_B T}(1-2\tilde{c}_s) - \ln c_s \tag{92}$$

Taking the inverse:

$$\gamma_s = \frac{1}{c_s}\frac{\tilde{c}_s}{1-\tilde{c}_s} e^{\frac{\Omega}{k_B T}(1-2\tilde{c}_s)} = \frac{1}{c_{s,max}-c_s} e^{\frac{\Omega}{k_B T}(1-2\tilde{c}_s)} \tag{93}$$

Using $\frac{\partial \ln y}{\partial \ln x} = \frac{\partial y}{\partial x}\frac{x}{y}$ we obtain:

$$\frac{\partial \ln \gamma_s}{\partial \ln c_s} = \frac{\partial \gamma_s}{\partial c_s}\frac{c_s}{\gamma_s} =$$
$$\left(\frac{-1}{(c_{s,max}-c_s)^2} e^{\frac{\Omega}{k_B T}(1-2\tilde{c}_s)} - \frac{-2}{(c_{s,max}-c_s)}\frac{\Omega}{k_B T c_{s,max}} e^{\frac{\Omega}{k_B T}(1-2\tilde{c}_s)}\right) c_s(c_{s,max}-c_s) e^{-\frac{\Omega}{k_B T}(1-2\tilde{c}_s)} \tag{94}$$

Which after simplifying becomes:

$$\frac{\partial \ln \gamma_s}{\partial \ln c_s} = -\frac{c_s}{c_{s,max} - c_s} - \frac{2_s}{k_B T c_{s,max}} = -\frac{\tilde{c}_s}{1 - \tilde{c}_s} - \frac{2\Omega \tilde{c}_s}{k_B T} \tag{95}$$

Plugging this result in to 91, the final mass balance equation is:

$$\frac{\partial c_s}{\partial t} = \nabla \cdot (D_{chem} \nabla c_s) \tag{96}$$

with

$$D_{chem} = D_0(1 - 2\tilde{\Omega}\tilde{c}_s + 2\tilde{\Omega}\tilde{c}_s^2) \tag{97}$$

When the general solution parameter is zero, Fick's law is recovered.

# B Solid diffusion model used by Landstorfer et al.

Instead of the proposed weak electrolyte model with interstitial and immobile lithium, the Landstorfer et al. implementation takes an approach similar to the solid particle model (Landstorfer, Funken, & Jacob, 2011). The starting assumption is modelling the solid as a lattice gas. Let $N$ be the number of particles and $N_{ls}$ the number of lattice sites, the filling fraction given by $x = \frac{N}{N_{ls}}$. The entropy of the system is given by

$$S = k_B \ln(\Omega) \tag{98}$$

with $\Omega$ the number of states of the system given by the binomial coefficient $\Omega = \binom{N_{ls}}{N} = \frac{N_{ls}!}{N!(N_{ls}-N)!}$. Through the use of Stirling's formula:

$$N! = N\ln(N) - N \tag{99}$$

for $N$ sufficiently large, we can write $S$ as

$$S = k_B \left[N_{ls}\ln(N_{ls}) - N\ln(N) - (N_{ls}-N)\ln(N_{ls}-N)\right] \tag{100}$$

We substitute $x = \frac{N}{N_{ls}}$ and divide through by $N_{ls}$ for the entropy density per site, and add and subtract the identical last two terms below that show the $N$ and $N_{ls}$ and be eliminated from the logarithm's arguments.

$$s = k_B \left[\ln(N_{ls}) + (x)\ln(N) - (1-x)\ln(N_{ls}-N) + (1-x)\ln(N_{ls}) - (1-x)\ln(N_{ls})\right] \tag{101}$$

Then we arrive at the entropy density per site in terms of $x$

$$s = k_B \left[x\ln(x) + (1-x)\ln(1-x)\right] \tag{102}$$

For the Gibbs free energy we use the identity

$$g = h - Ts + zex\phi \tag{103}$$

We replace the enthalpy density $h$ by a mixing energy $\zeta x(1-x)$ accounting for the deviation from ideal mixing due to particle-particle interactions. This term is similar to the entropy of mixing term in the solid particle model. At constant $T$, $P$ and $\phi$, the electrochemical potential per particle is given by

$$\mu = \left(\frac{\Delta G}{\Delta N}\right)_{T,P,\phi} = \left(\frac{\partial g}{\partial x}\right)_{T,P,\phi} \tag{104}$$

so we have

$$\begin{aligned}\mu &= \frac{\partial}{\partial x}\Big(\zeta x(1-x) - k_B T\left[x\ln(x) + (1-x)\ln(1-x)\right] + zex\phi\Big) \\ &= \zeta(1-2x) - k_B T \ln\left(\frac{x}{1-x}\right) + ze\phi\end{aligned} \tag{105}$$

At this point the filling fraction can be replaced by the dimensionless concentration $\tilde{c} = \frac{c}{c_{max}}$.Calculating the mass flux gives rise to the special diffusion coefficient that is the result of the assumption of a lattice gas with energy of mixing:

$$F = -Mc\nabla\mu = Mk_B T\left(\frac{1}{1-c} - \zeta 2c\right)\nabla c - Mc\nabla\phi \tag{106}$$

The $c$ dependency of the diffusion coefficient comes from the fact that the ability for a particle to move to another lattice site is dependent on the number of occupied lattices sites in a neighbourhood around the particle.

# C Values used in simple porous electrode model

| Symbol | Variable | Value | Unit |
|---|---|---|---|
| $L_e$ | Electrolyte/separator length | $25 \cdot 10^{-6}$ | m |
| $L_c$ | Cathode length | $50 \cdot 10^{-6}$ | m |
| $\epsilon$ | Cathode porosity | 0.4 | - |
| $R$ | Particle length | $100 \cdot 10^{-9}$ | m |
| $a_p$ | Particle surface area per unit volume | $\frac{2R^2}{R^3} = 2 \cdot 10^7$ | $\frac{\mathrm{m}^2}{\mathrm{m}^3}$ |
| $D_+$ | Lithium diffusion coefficient (liquid electrolyte) | $2.2 \cdot 10^{-10}$ | $\frac{\mathrm{m}^2}{\mathrm{s}}$ |
| $D_+$ | Electron diffusion coefficient (liquid electrolyte) | $2.94 \cdot 10^{-10}$ | $\frac{\mathrm{m}^2}{\mathrm{s}}$ |
| $D_0$ | Active particle diffusity | $3.3 \cdot 10^{-15}$ | $\frac{\mathrm{m}^2}{\mathrm{s}}$ |
| $\boldsymbol{i}_0$ | Exchange current density | 1.0 | $\frac{C}{\mathrm{m}^2}$ |
| $\Omega$ | General solution parameter | $3k_BT$ | joule |

# 6 References


Bachman, J. C., Muy, S., Grimaud, A., Chang, H.-H., Pour, N., Lux, S. F., ... Shao-Horn, Y. (2015, December). Inorganic solid-state electrolytes for lithium batteries: Mechanisms and properties governing ion conduction. *Chemical Reviews*, *116*(1), 140–162. Retrieved from https://doi.org/10.1021/acs.chemrev.5b00563

Balluffi, R. W., Allen, S. M., & Carter, W. C. (2005). *Kinetics of materials*. John Wiley & Sons, Inc. Retrieved from https://doi.org/10.1002/0471749311

Bazant, M. Z. (2012). Phase-field theory of ion intercalation kinetics. , A1967–A1985.

Cahn, J. W., & Hilliard, J. E. (1958, February). Free energy of a nonuniform system. i. interfacial free energy. *The Journal of Chemical Physics*, *28*(2), 258–267. Retrieved from https://doi.org/10.1063/1.1744102

Ingram, M., Moynihan, C., & Lesikar, A. (1980, May). Ionic conductivity and the weak electrolyte theory of glass. *Journal of Non-Crystalline Solids*, *38-39*, 371–376. Retrieved from https://doi.org/10.1016/0022-3093(80)90447-0

Kan, J. (2019). *Numerical methods for partial differential equations*. Delft: Delft Academic Press.

Kobayashi, T., Yamada, A., & Kanno, R. (2008, June). Interfacial reactions at electrode/electrolyte boundary in all solid-state lithium battery using inorganic solid electrolyte, thio-LISICON. *Electrochimica Acta*, *53*(15), 5045–5050. Retrieved from https://doi.org/10.1016/j.electacta.2008.01.071

Landstorfer, M., Funken, S., & Jacob, T. (2011). An advanced model framework for solid electrolyte intercalation batteries. *Physical Chemistry Chemical Physics*, *13*(28), 12817. Retrieved from https://doi.org/10.1039/c0cp02473b

Liu, C., Neale, Z., & Cao, G. (2016, 03). Understanding electrochemical potentials of cathode materials in rechargeable batteries. *Materials Today*, *19*, 109-123.

Minami, T. (2005). *Solid state ionics for batteries*. Tokyo New York: Springer.

Moelans, N., Blanpain, B., & Wollants, P. (2008, June). An introduction to phase-field modeling of microstructure evolution. *Calphad*, *32*(2), 268–294. Retrieved from https://doi.org/10.1016/j.calphad.2007.11.003

Monroe, C., & Newman, J. (2007, 09). An introduction to the onsager reciprocal relations. , *41*, 233-238.

Newman, J. (2004). *Electrochemical systems*. Hoboken, N.J: J. Wiley.

Park, M., Zhang, X., Chung, M., Less, G. B., & Sastry, A. M. (2010, December). A review of conduction phenomena in li-ion batteries. *Journal of Power Sources*, *195*(24), 7904–7929. Retrieved from https://doi.org/10.1016/j.jpowsour.2010.06.060

Provatas, N., & Elder, K. (2010). *Phase-field methods in materials science and engineering*. Wiley-VCH Verlag GmbH & Co. KGaA. Retrieved from https://doi.org/10.1002/9783527631520

Qin, R. S., & Bhadeshia, H. K. (2010, July). Phase field method. *Materials Science and Technology*, *26*(7), 803–811. Retrieved from https://doi.org/10.1179/174328409x453190

Raijmakers, L., Danilov, D., Eichel, R.-A., & Notten, P. (2020, January). An advanced all-solid-state li-ion battery model. *Electrochimica Acta*, *330*, 135147. Retrieved from https://doi.org/10.1016/j.electacta.2019.135147

Smith, R. B., & Bazant, M. Z. (2017). Multiphase porous electrode theory. *Journal of The Electrochemical Society*, *164*(11), E3291–E3310. Retrieved from https://doi.org/10.1149/2.0171711jes

Wu, M., Xu, B., & Ouyang, C. (2016, January). Physics of electron and lithium-ion transport in electrode materials for li-ion batteries. *Chinese Physics B*, *25*(1), 018206. Retrieved from

https://doi.org/10.1088/1674-1056/25/1/018206

Zheng, F., Kotobuki, M., Song, S., Lai, M. O., & Lu, L. (2018, June). Review on solid electrolytes for all-solid-state lithium-ion batteries. *Journal of Power Sources*, *389*, 198–213. Retrieved from https://doi.org/10.1016/j.jpowsour.2018.04.022